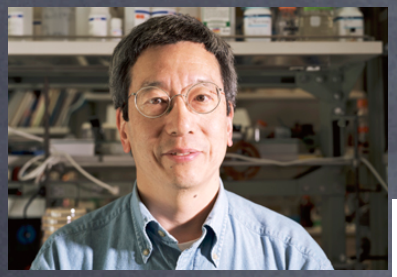

hhmi | Howard Hughes Medical Institute

Nobel Lectures

R. Y. Tsien

DOI: 10.1002/anie.200901916

Green Fluorescent Protein

Constructing and Exploiting the Fluorescent Protein Paintbox (Nobel Lecture)**

*Roger Y. Tsien**

FLUORESCENCE READOUTS OF BIOCHEMISTRY IN LIVE CELLS AND ORGANISMS

ROGER Y. TSIEN, PHD

GFP - Green Fluorescent Protein

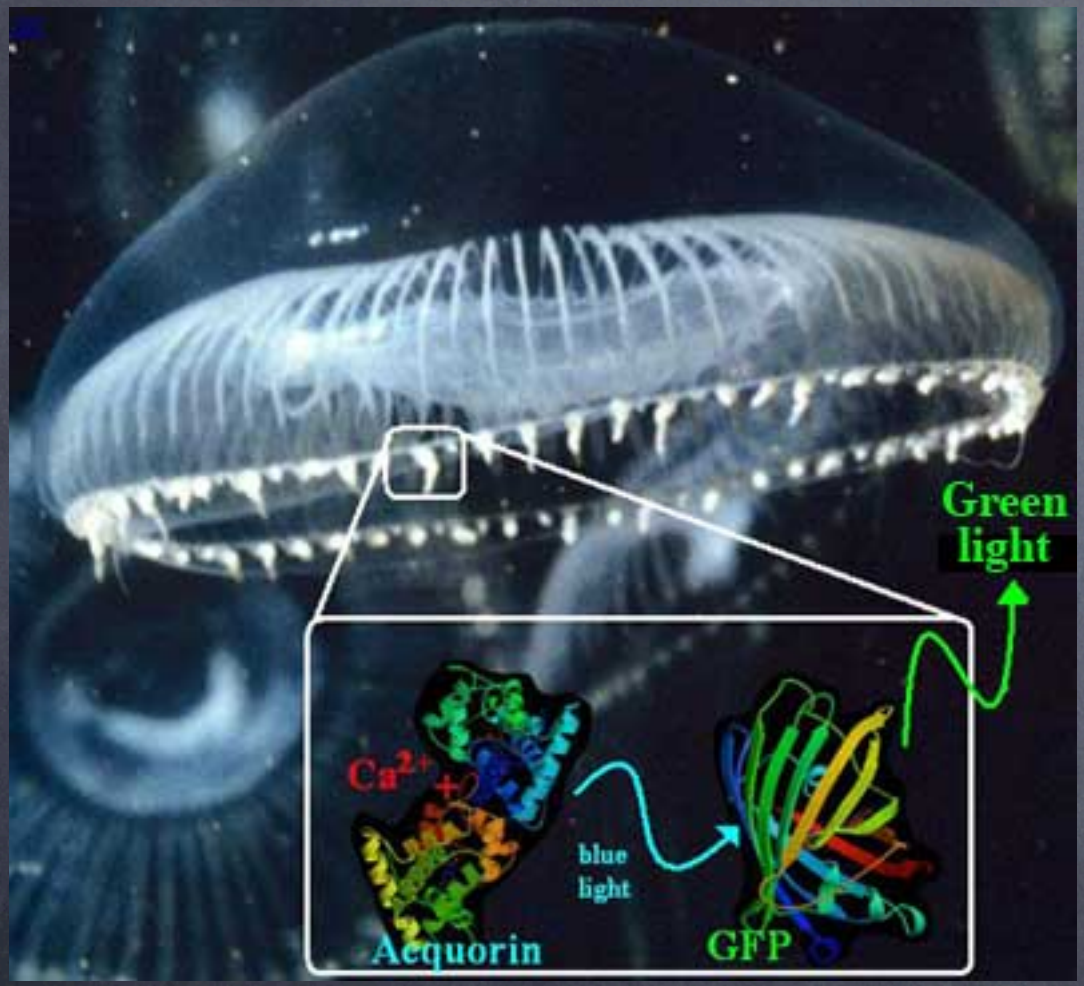

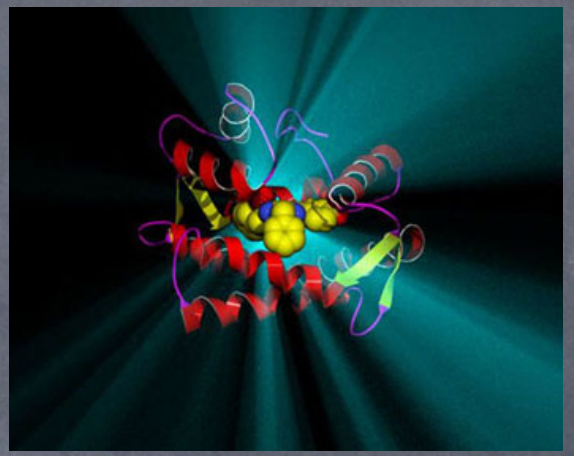

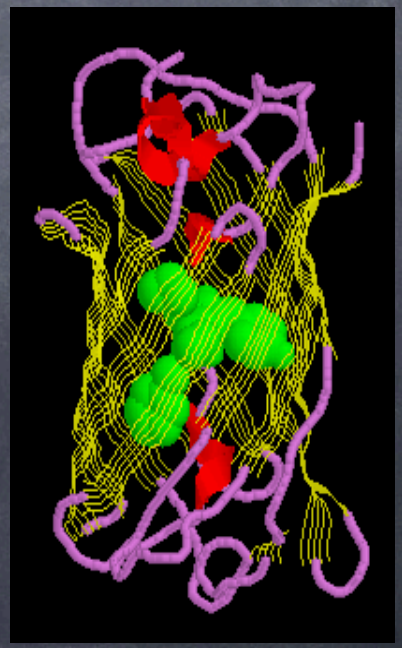

Aequoria Victoria

- Discovered 1962 as companion to aequorin
- Cloned 1992, expression 1994
- 238 Aminoacids
- 27-30 kDa
- Fluorophore made by 3 aminoacids (65-67) "protected" in a cylinder

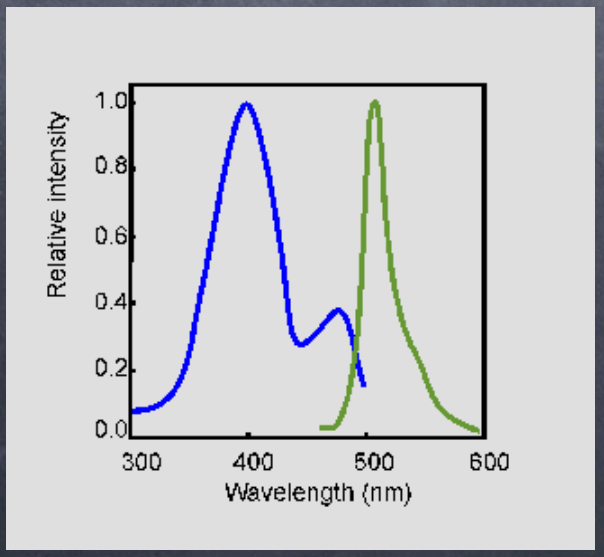

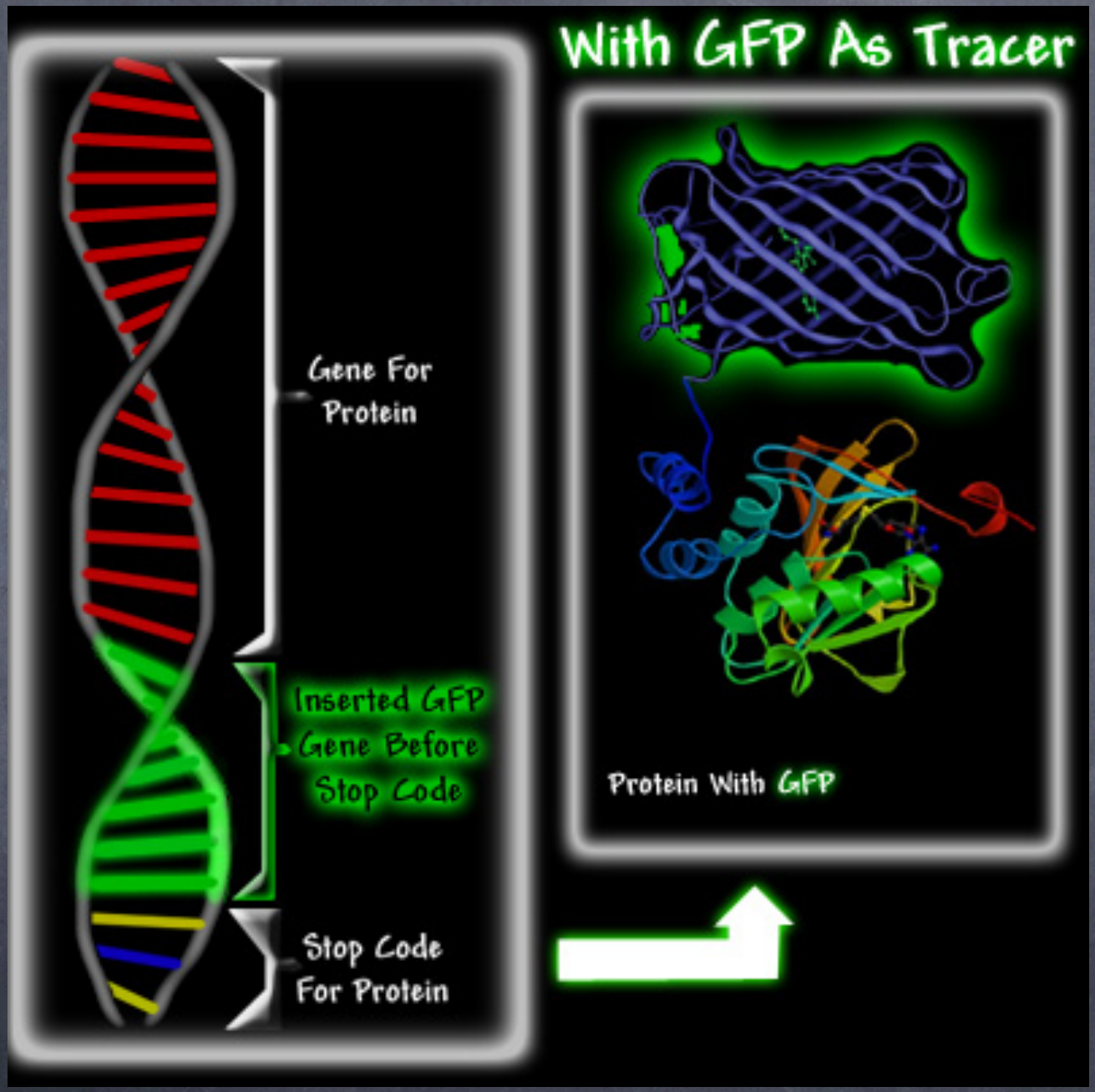
With GFP As Tracer
Gene For Protein
Inserted GFP Gene Before Stop Code
Stop Code For Protein
Protein With GFP

GFPs

- Blue BFP
- Cyan CFP
- Green GFP
- Yellow YFP
- Red DsRed
  HcRed
- GFP timer

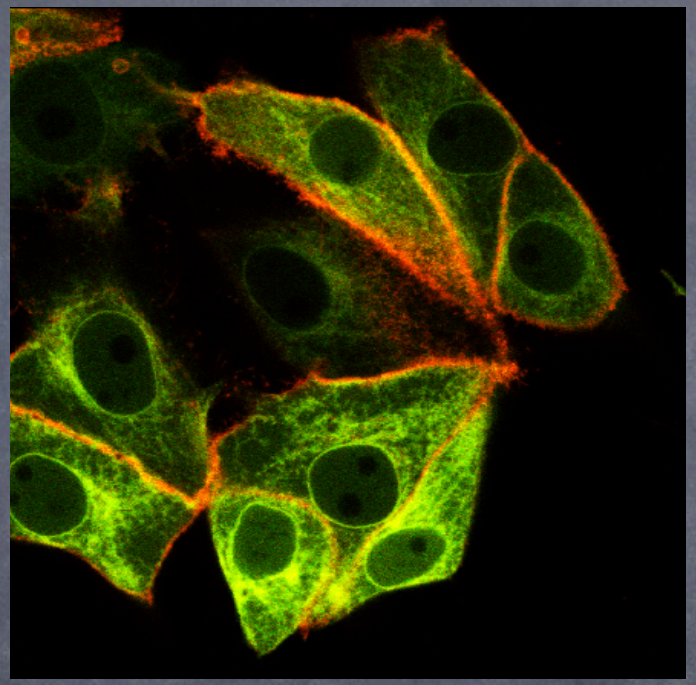

CFP
GFP

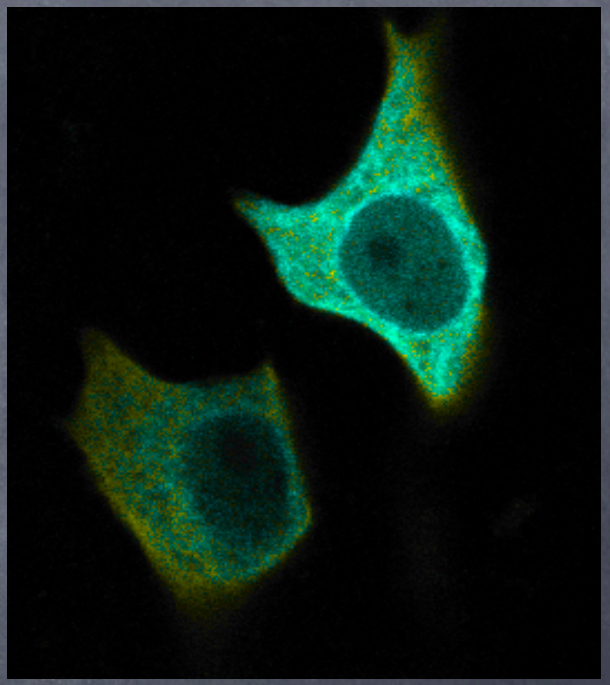

CFP
YFP

Fluorescence Resonance Energy Transfer (FRET)

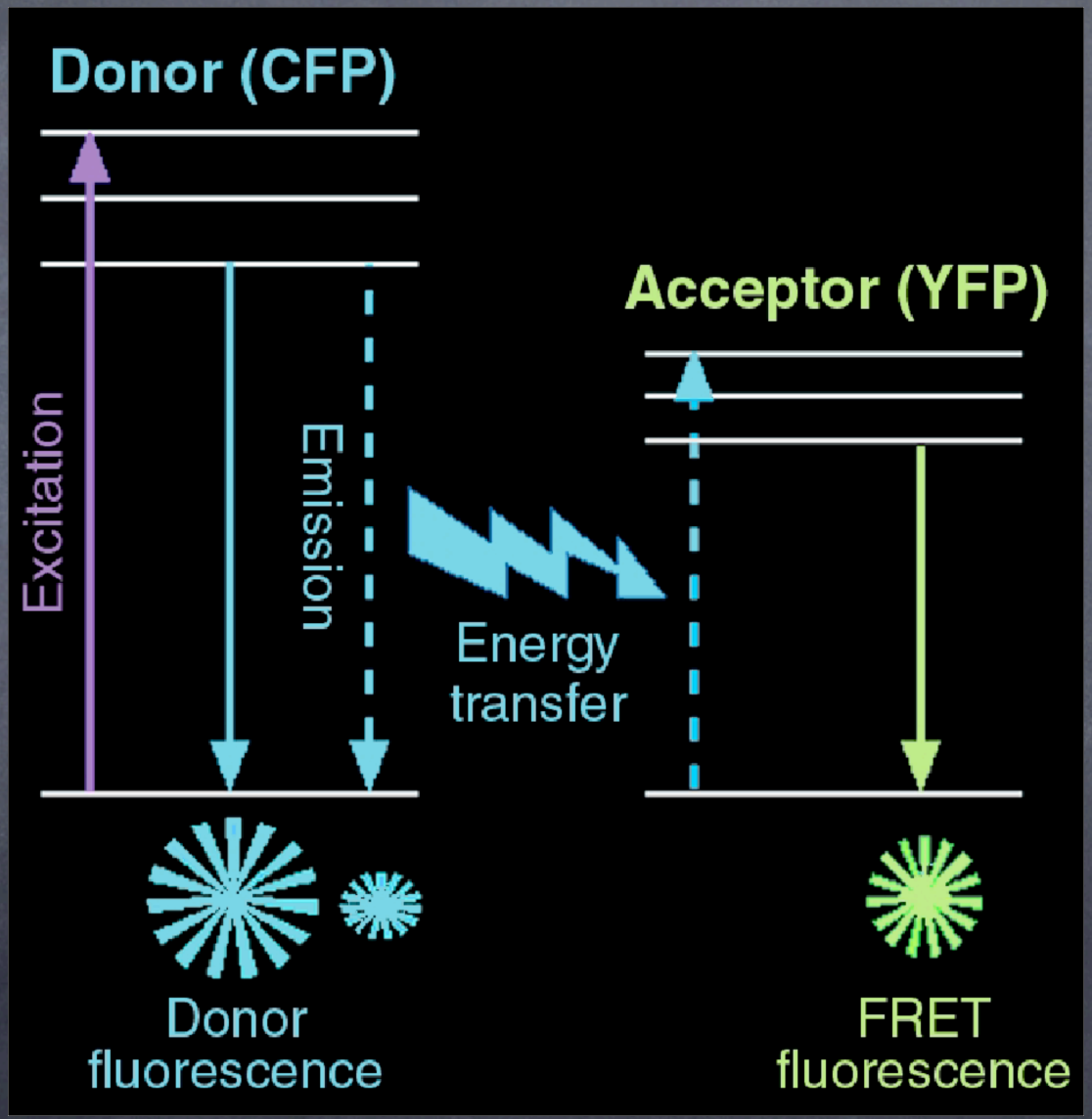

L'efficienza di FRET dipende da molti fattori

$$E = \frac{k_{ET}}{k_f + k_{ET} + \sum k_i}$$

The FRET efficiency is the quantum yield of the energy transfer transition, i.e. the fraction of energy transfer event occurring per donor excitation event

in cui

k_{ET} =rate of energy transfer

k_f =radiative decay rate

k_i = rate constants of any other de-excitation pathways

$$E = 1 - \frac{F'_D}{F_D} \quad \text{or} \quad E = 1 - \frac{\tau'_D}{\tau_D}$$

F_D e F'_D fluorescence intensity of donor in the absence or presence of acceptor

τ_D e τ'_D fluorescence lifetime of donor in the absence or presence of acceptor

$$E = \frac{1}{1 + (\frac{r}{R_0})^6}$$

r = distance between donor and acceptor

R_0^6 = Forster distance=$8.8 * 10^{23} k^2 n^{-4} Q_0 J$

k^2 = dipole orientation factor

Q_0 = fluorescence quantum yield of the donor in the absence of the acceptor

n=refractive index

J=spectral overlap

$$J = \int f_D(\lambda) \varepsilon_A(\lambda) \lambda^4 \, d\lambda$$

f_D = donor emission spectrum normalized

ε_A = acceptor molar extinction coefficient

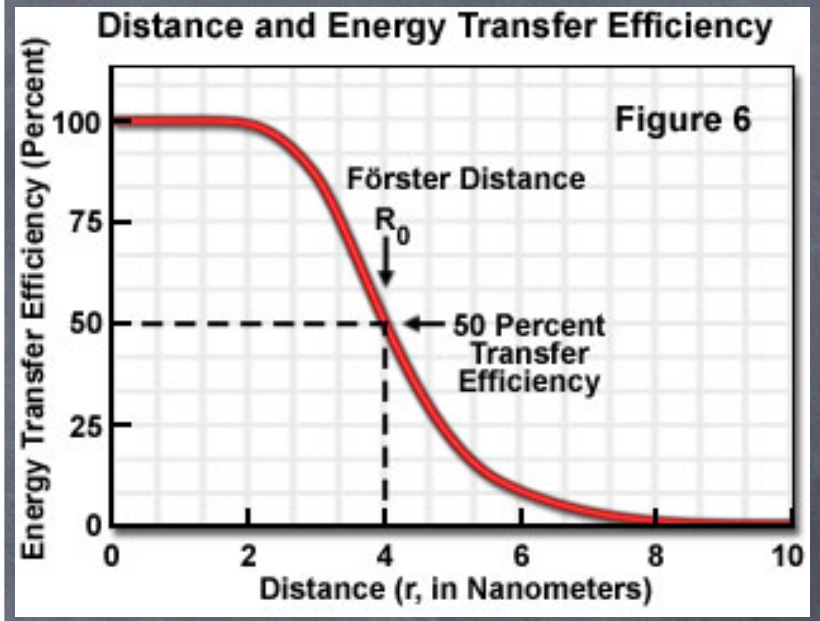

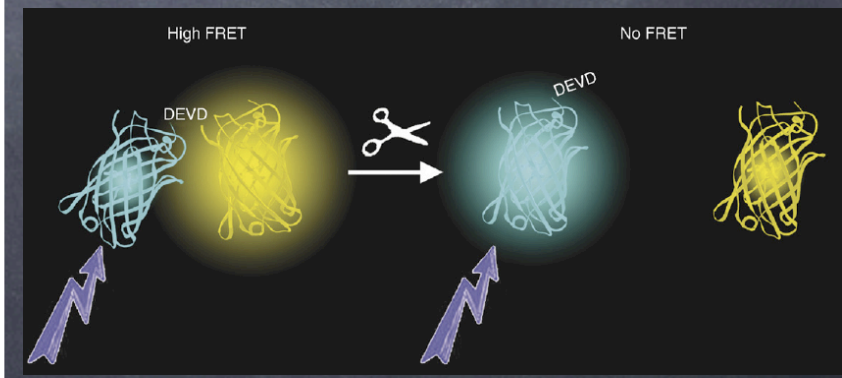

Fluorescence lifetime

Average time at which a molecule stays in excited state before photon emission

$$[S1] = [S1]_0^{-\Gamma t}$$

$$\Gamma = \frac{1}{\text{fluorescence lifetime}} = \text{decay rate}$$

$$\Gamma_{tot} = \Gamma_{rad} + \Gamma_{nonrad}$$

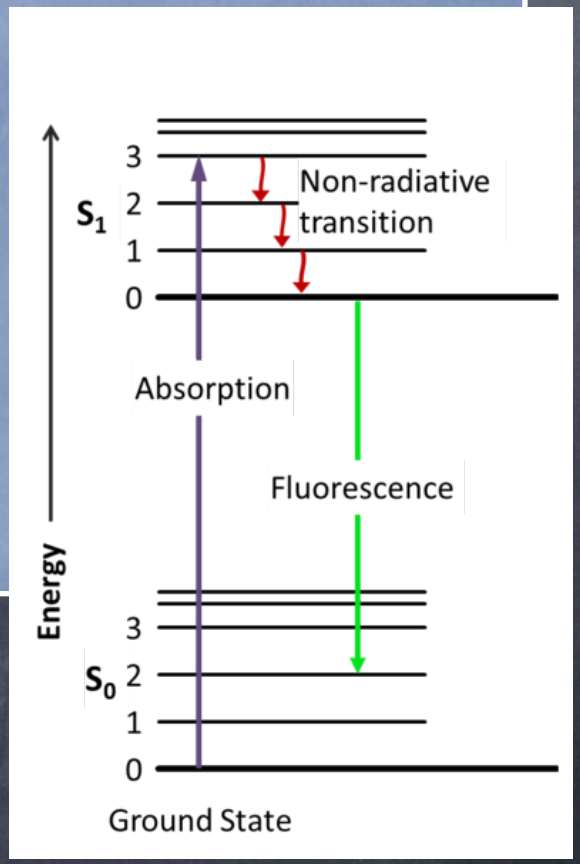

Fluorescence lifetime imaging (FLIM-FRET)

More FRET, shorter donor fluorescence lifetime

No need to measure fluorescence

$$E = 1 - \frac{\tau'_D}{\tau_D}$$

FRET allows to follow protein-protein interaction in vivo

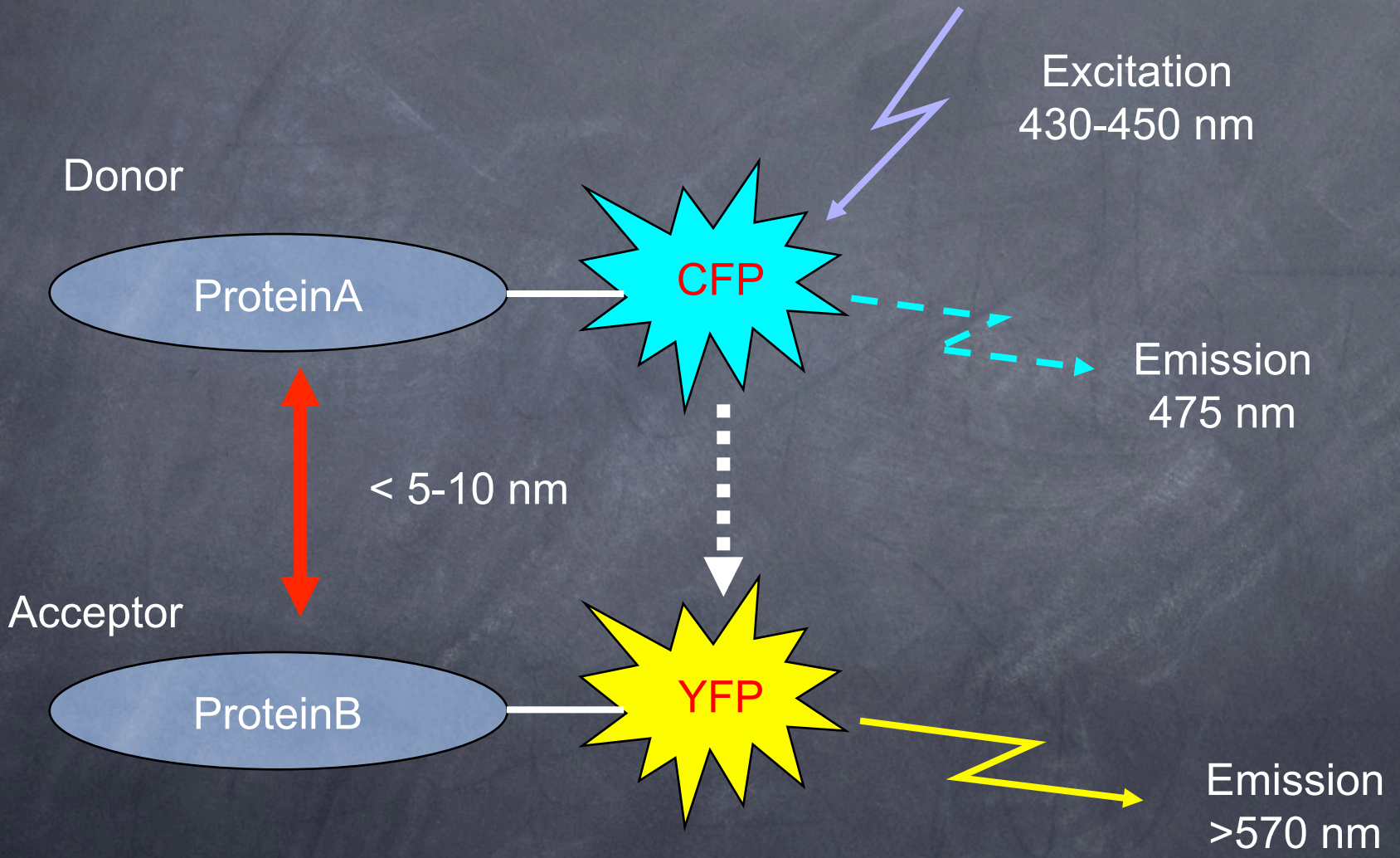

THE JOURNAL OF BIOLOGICAL CHEMISTRY VOL. 285, NO. 10, pp. 7818–7826, March 5, 2010
© 2010 by The American Society for Biochemistry and Molecular Biology, Inc. Printed in the U.S.A.

The Scaffold Protein Shoc2/SUR-8 Accelerates the Interaction of Ras and Raf*[S]

Received for publication, August 9, 2009, and in revised form, December 19, 2009 Published, JBC Papers in Press, January 5, 2010, DOI 10.1074/jbc.M109.053975

Rie Matsunaga-Udagawa[‡1], Yoshihisa Fujita[‡1], Sayaka Yoshiki[‡], Kenta Terai[‡2], Yuji Kamioka[§], Etsuko Kiyokawa[§], Katsuyuki Yugi[¶], Kazuhiro Aoki[‡‖3], and Michiyuki Matsuda[‡§]

From the [‡]Laboratory of Bioimaging and Cell Signaling, Graduate School of Biostudies, and the [§]Department of Pathology and Biology of Diseases, Graduate School of Medicine, Kyoto University, Kyoto 606-8501, the [¶]Department of Biosciences and Informatics, Keio University, Kanagawa 223-8522, and [‖]PREST, Japan Science and Technology Agency (JST), 4-1-8 Honcho, Kawaguchi, Saitama 332-0012, Japan

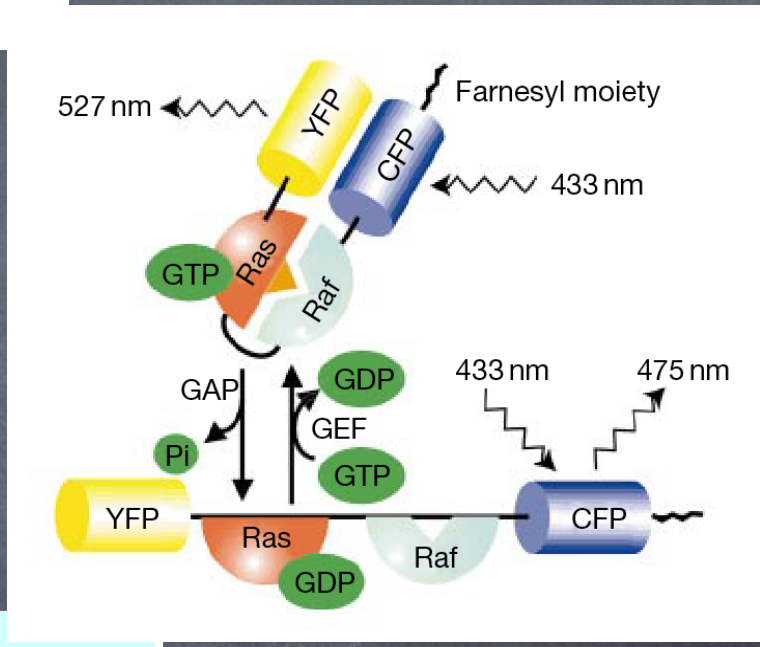

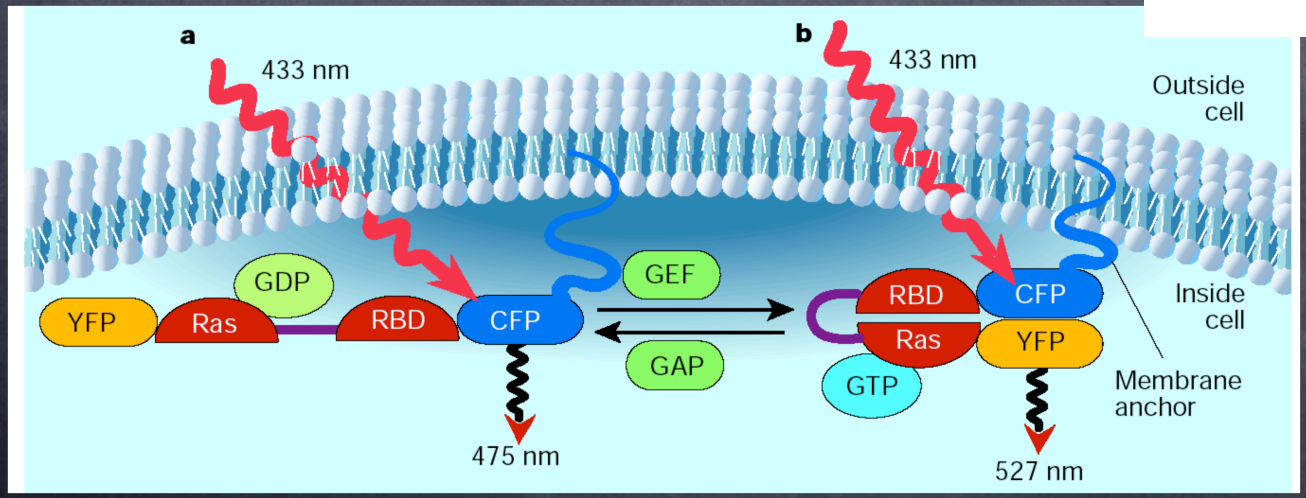

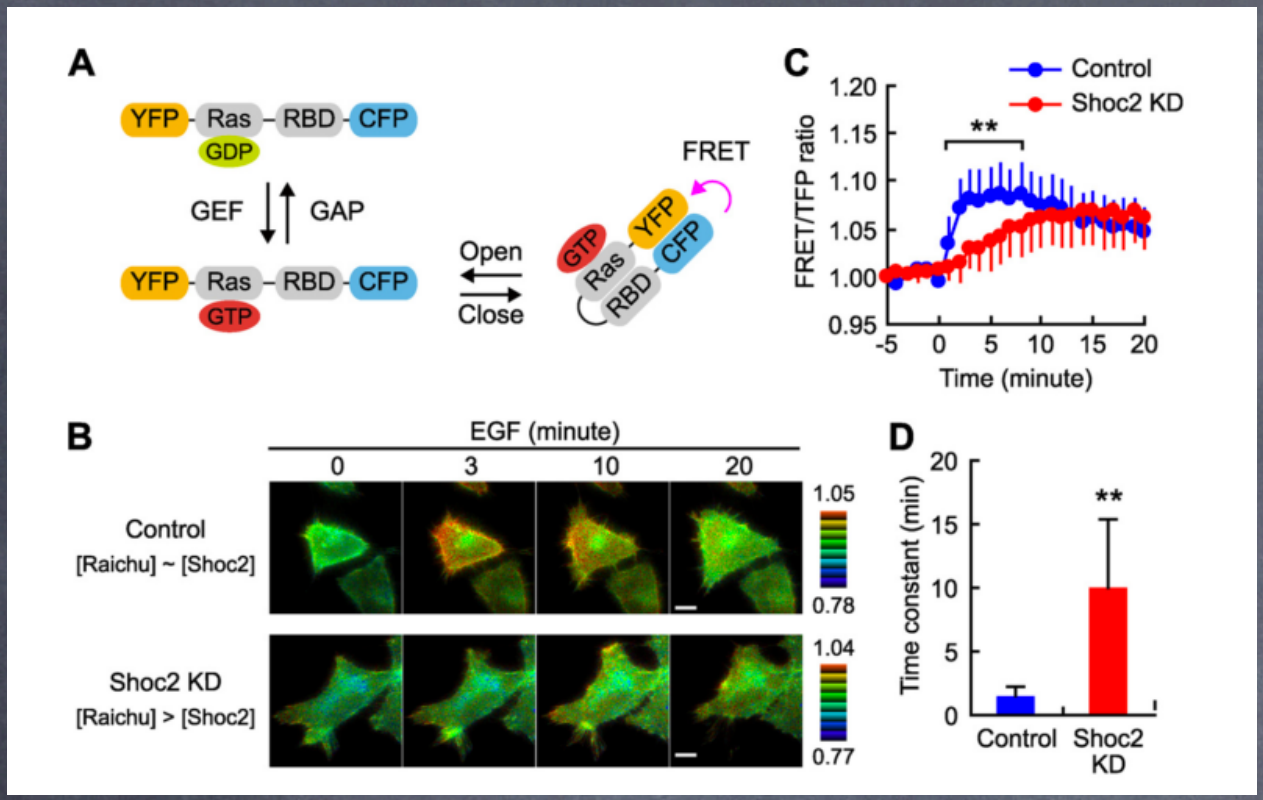

FIGURE 3. **Effect of Shoc2 knockdown (*KD*) on the activation of Ras detected by FRET imaging.** *A*, a schematic model of Raichu-Ras is shown. Within the probe, Ras is activated by GEF followed by association of Raf-RBD. *B*, HeLa cells stably expressing Raichu-Ras were transfected with control (*upper*) or Shoc2-targeted siRNA (*lower*). Two days later, the cells were starved for 6 h. Then, images were obtained every 1 min for 30 min after stimulation with 1.0 ng/ml of EGF. Representative ratio images of FRET/TFP at the indicated time points after EGF addition (in minutes) are shown in the intensity-modulated display mode. In the intensity-modulated display mode, eight colors from red to blue are used to represent the FRET/TFP ratio, with the intensity of each color indicating the mean intensity of FRET and TFP. The *upper* and *lower* limits of the ratio range are shown on the *right*. *Bars*, 10 μm. *C*, the relative FRET/TFP ratios normalized by the average FRET/TFP before stimulation were plotted until 20 min after EGF addition with the S.D. The *blue* and *red lines* indicate control and Shoc2-depletion, respectively. The *symbols* indicate the results of *t* test analysis; **, $p < 0.01$ compared with the control. *D*, the *bar graph* represents the average of the time constants in control cells ($n = 32$) or that in Shoc2-knockdown cells ($n = 19$). The *symbol* shows the results of *t* test analysis; **, $p < 0.01$ compared with the control. *E*, HeLa cells were transfected with expression plasmids of Raichu-Ras-WT or Raichu-Ras-V12, and GST or GST-Shoc2. Forty-eight hours after transfection, the cells were lysed and pulled down by glutathione beads. The cell lysates (*left*) and eluates (*right*) were subjected to immunoblot analysis with antibodies against GFP and GST as indicated. Experiments were repeated three times, and the representative blots are shown. *F*, HeLa cells expressing EGFP-K-Ras-V12 and GST or GST-Shoc2 were lysed and pulled down by glutathione beads as in *E*. The cell lysates (*left*) and eluates (*right*) were subjected to immunoblot analysis with antibodies against GFP and GST as indicated. Experiments were repeated two times, and representative blots are shown.

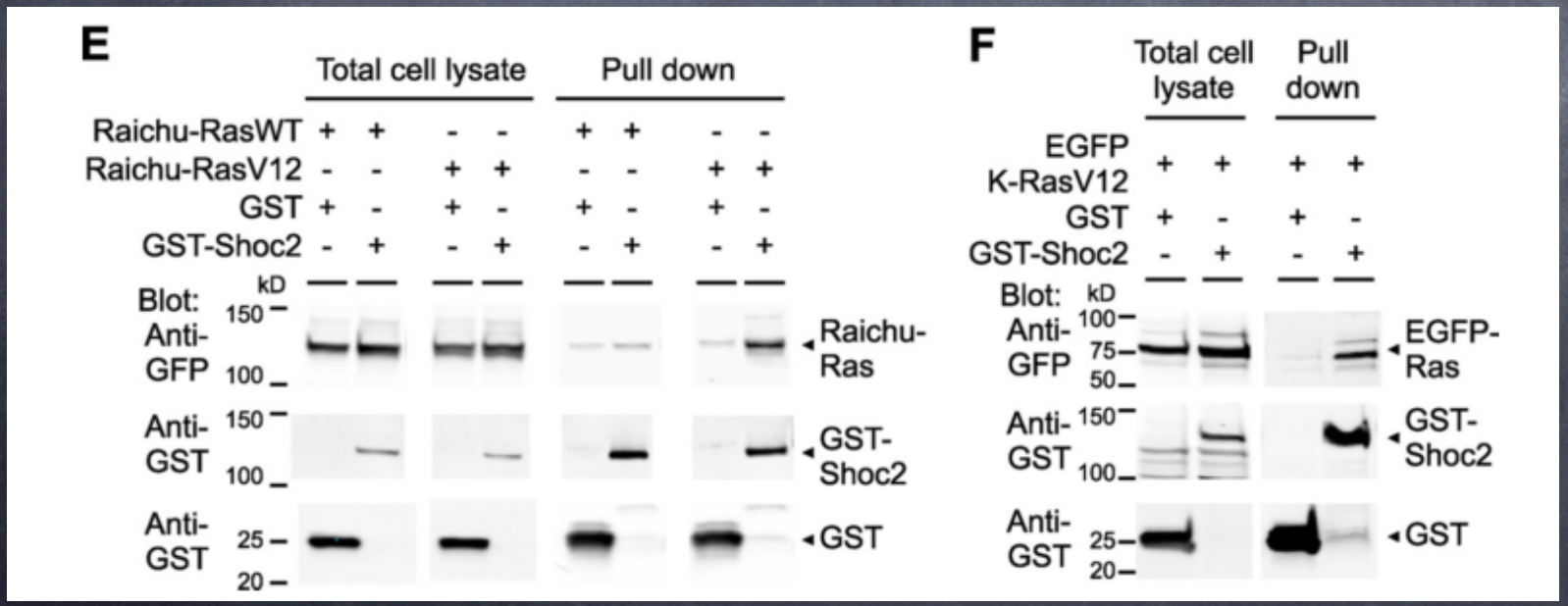

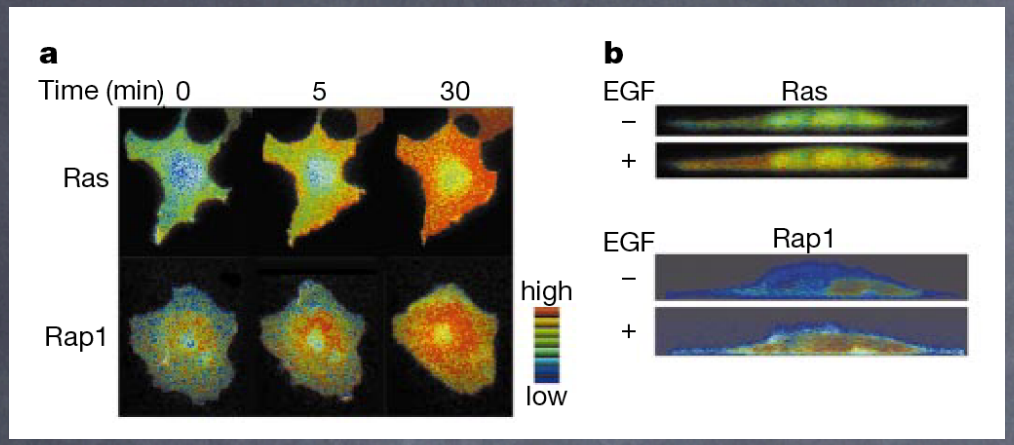
a
Time (min) 0
5
30
Ras
Rap1
high
low
b
EGF
Ras
–
+
EGF
Rap1
–
+

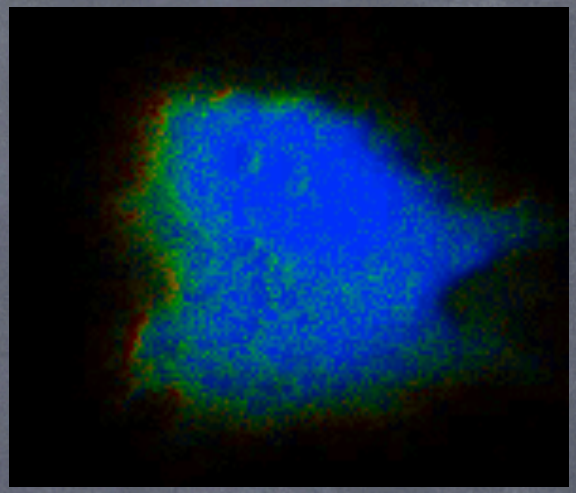

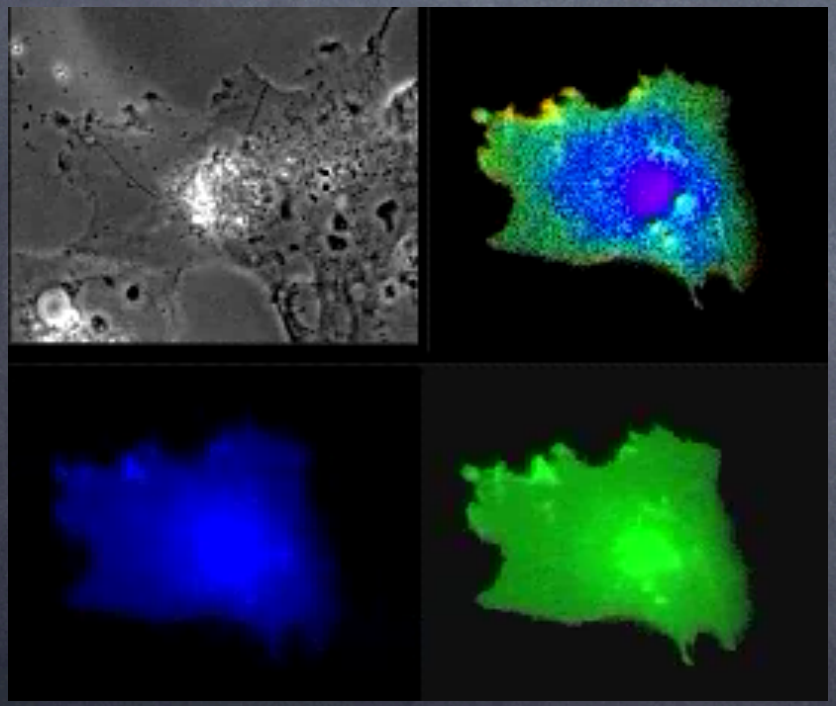

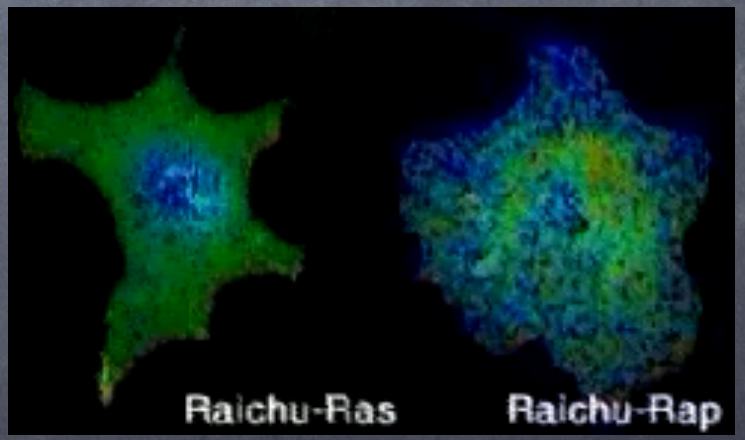
Raichu-Ras
Raichu-Rap

THE JOURNAL OF BIOLOGICAL CHEMISTRY
Vol. 278, No. 50, Issue of December 12, pp. 50355–50361, 2003
Printed in U.S.A.
© 2003 by The American Society for Biochemistry and Molecular Biology, Inc.

Cell Signaling Microdomain with Na,K-ATPase and Inositol 1,4,5-Trisphosphate Receptor Generates Calcium Oscillations*

Received for publication, May 22, 2003, and in revised form, August 20, 2003
Published, JBC Papers in Press, August 28, 2003, DOI 10.1074/jbc.M305378200

Ayako Miyakawa-Naito‡, Per Uhlén‡, Mark Lal, Oleg Aizman, Katsuhiko Mikoshiba§, Hjalmar Brismar, Sergey Zelenin, and Anita Aperia¶

From the Department of Woman and Child Health, Karolinska Institutet, Astrid Lindgren Children's Hospital, S-171 76 Stockholm, Sweden and the §Department of Basic Medical Science, The Institute of Medical Science, The University of Tokyo, 4-6-1 Shirokanedai, Minato-ku, Tokyo 108-8639, Japan

Recent studies indicate novel roles for the ubiquitous ion pump, Na,K-ATPase, in addition to its function as a key regulator of intracellular sodium and potassium concentration. We have previously demonstrated that ouabain, the endogenous ligand of Na,K-ATPase, can trigger intracellular Ca^{2+} oscillations, a versatile intracellular signal controlling a diverse range of cellular processes. Here we report that Na,K-ATPase and inositol 1,4,5-trisphosphate ($InsP_3$) receptor ($InsP_3R$) form a cell signaling microdomain that, in the presence of ouabain, generates slow Ca^{2+} oscillations in renal cells. Using fluorescent resonance energy transfer (FRET) measurements, we detected a close spatial proximity between Na,K-ATPase and $InsP_3R$. Ouabain significantly enhanced FRET between Na,K-ATPase and $InsP_3R$. The FRET effect and ouabain-induced Ca^{2+} oscillations were not observed following disruption of the actin cytoskeleton. Partial truncation of the NH_2 terminus of Na,K-ATPase catalytic α1-subunit abolished Ca^{2+} oscillations and downstream activation of NF-κB. Ouabain-induced Ca^{2+} oscillations occurred in cells expressing an $InsP_3$ sponge and were hence independent of $InsP_3$ generation. Thus, we present a novel principle for a cell signaling microdomain where an ion pump serves as a receptor.

FRET between proteins on different membranes

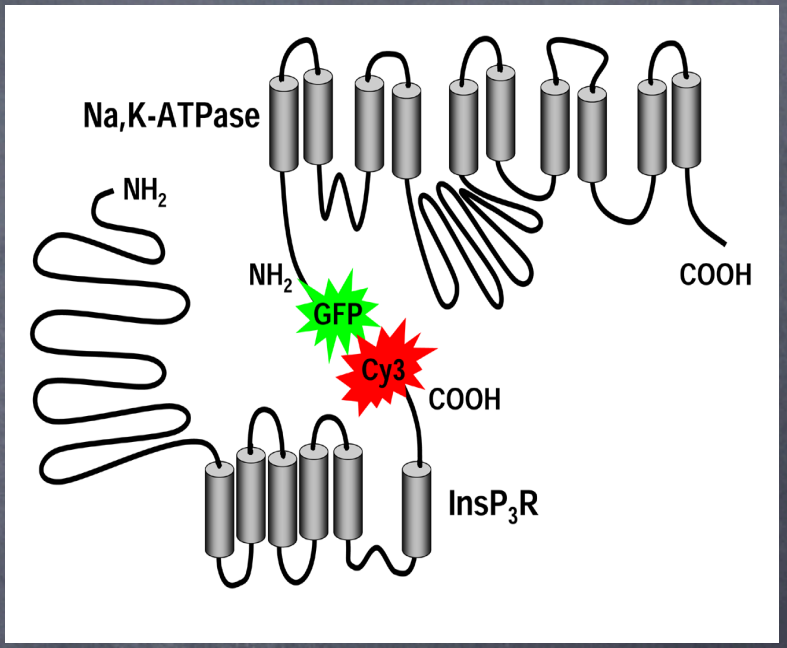

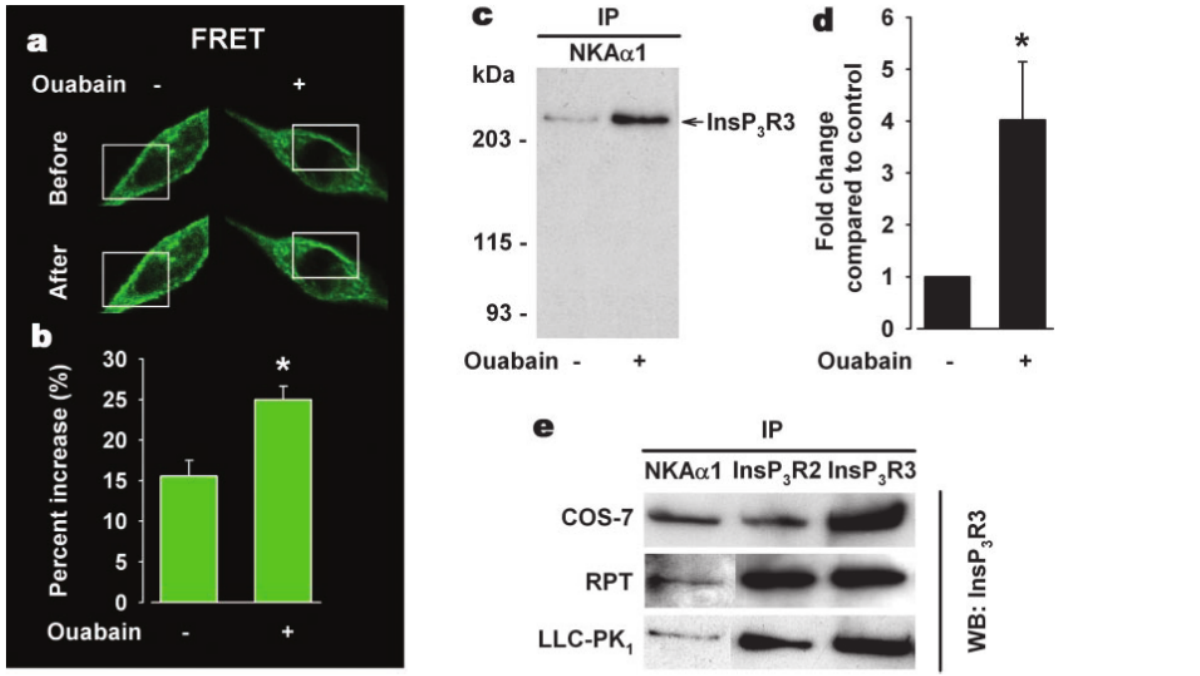

FIG. 3. **Studies of Na,K-ATPase and $InsP_3R$ signaling microdomain.** *a* and *b*, FRET measurements between Na,K-ATPase and $InsP_3R3$. *a*, GFP-NKAα1 images of COS-7 cells with and without ouabain treatment before and after acceptor photobleaching (bleached area indicated by *square*). *b*, quantitative changes in emission intensities after bleaching as compared with before bleaching, mean ± S.E., *, $p < 0.05$. FRET was enhanced by ouabain. *c–e*, co-immunoprecipitation (*IP*) studies followed by Western blotting (*WB*) for $InsP_3R3$. *c* and *d*, representative Western blot (*c*) and densitometric analysis (*d*) of $InsP_3R3$ content in Na,K-ATPase immunoprecipitates before and after 250 μM ouabain treatment for 30 min in COS-7 cells. Ouabain significantly increased the amount of $InsP_3R3$ associated with Na,K-ATPase, mean ± S.E. ($n = 3$), *, $p < 0.05$. Molecular mass markers are indicated to the *left* of the blot. In *e*, $InsP_3R3$ co-immunoprecipitated with Na,K-ATPase and $InsP_3R2$ in COS-7, RPT and $LLC\text{-}PK_1$ cells.

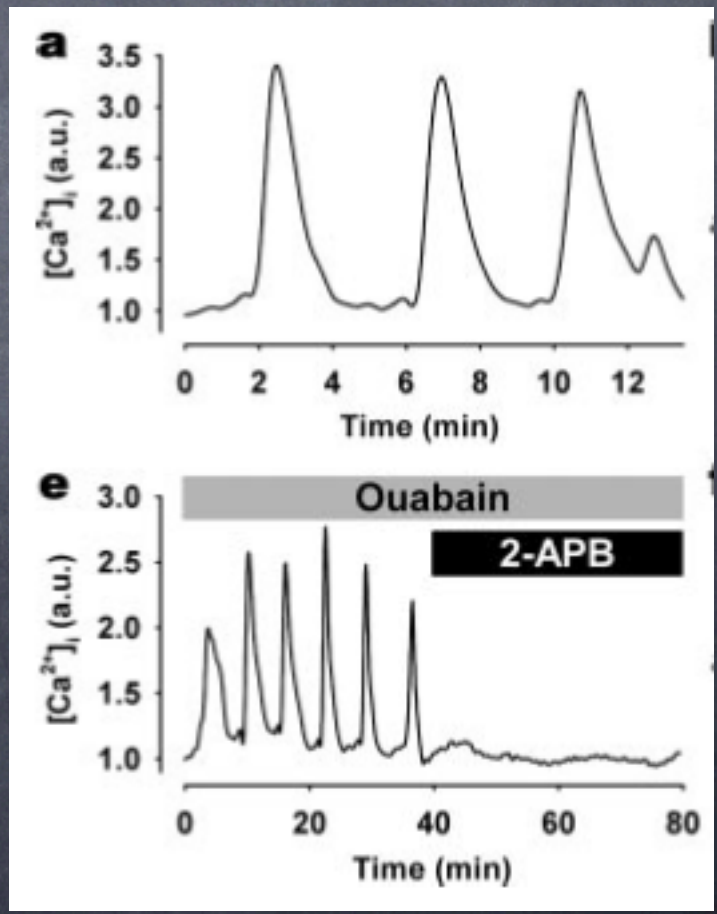

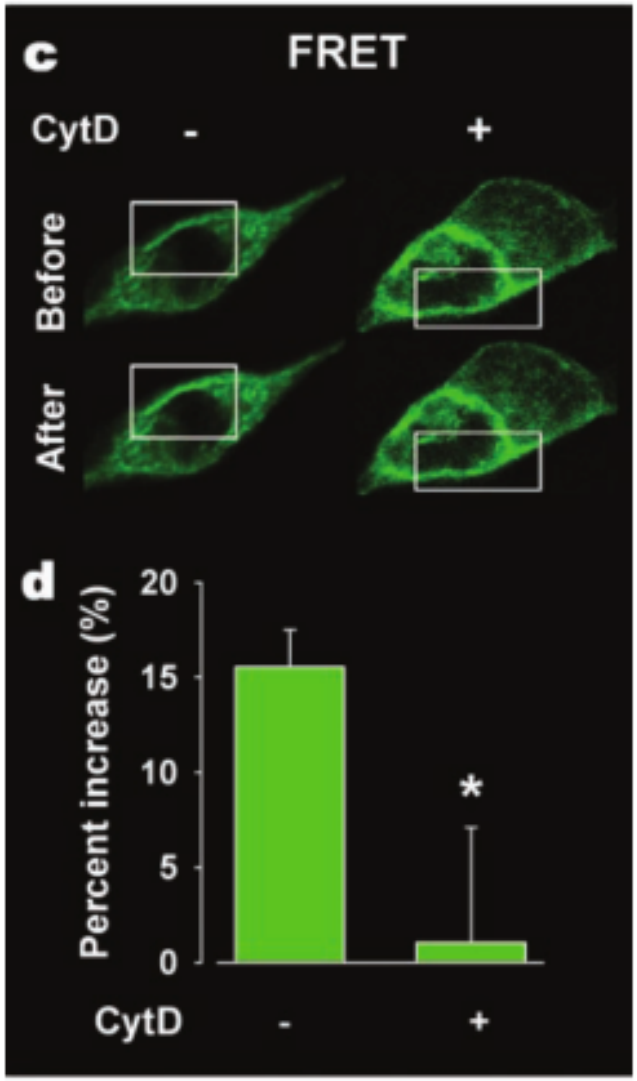

FIG. 4. **Effect of cytoskeleton perturbation on physical association between Na,K-ATPase and $InsP_3R$.** In *a*, the actin cytoskeleton was disrupted after CytD (5 μM) treatment in GFP-actin-expressing RPT cells. In *b*, CytD abolished ouabain-induced Ca^{2+} oscillations in RPT cells. Arbitrary units (*a.u.*) represent ratio values corresponding to intracellular Ca^{2+} concentration changes. *c* and *d*, FRET measurements between Na,K-ATPase and $InsP_3R3$. *c*, GFP-NKAα1 images of COS-7 cells with and without CytD treatment before and after acceptor photobleaching (bleached area indicated by *square*). *d*, quantitative changes in emission intensities after bleaching as compared with before bleaching, mean ± S.E., *, $p < 0.05$. FRET was eliminated by CytD. *e*, co-immunoprecipitation (*IP*) studies followed by Western blotting (*WB*) for $InsP_3R3$ in CytD-treated COS-7 cells. $InsP_3R3$ did not co-immunoprecipitate with Na,K-ATPase.

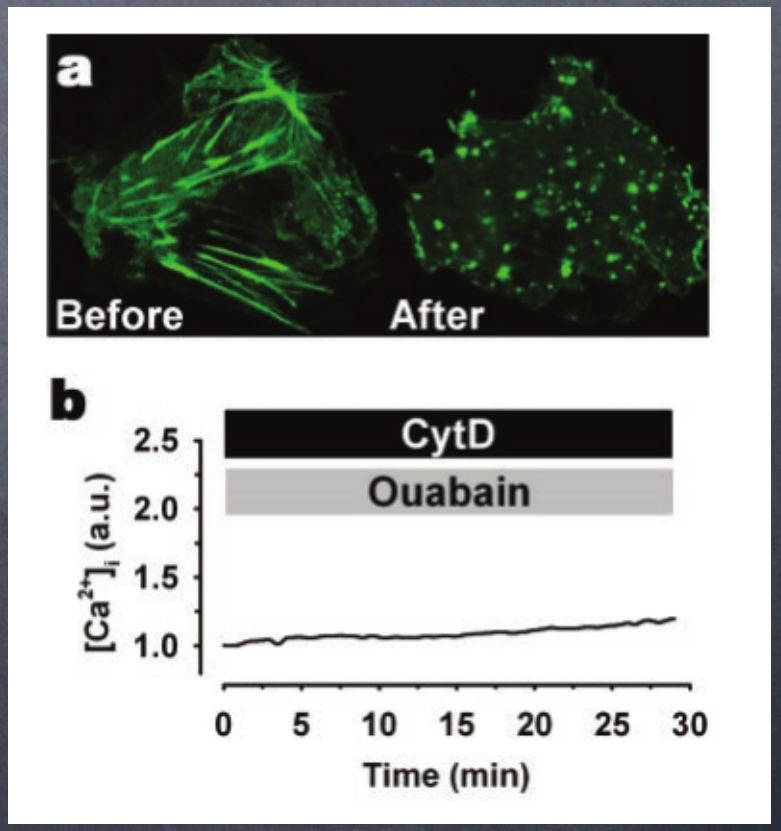

Intramolecular FRET : calcium sensors

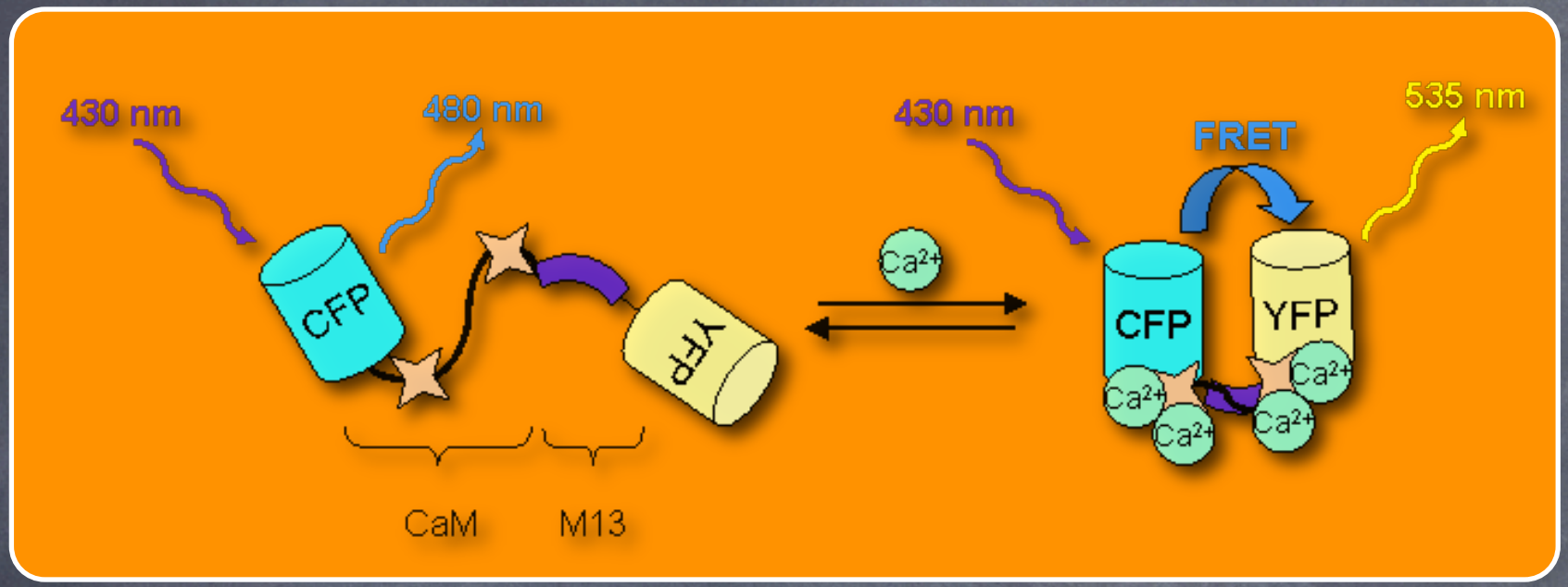

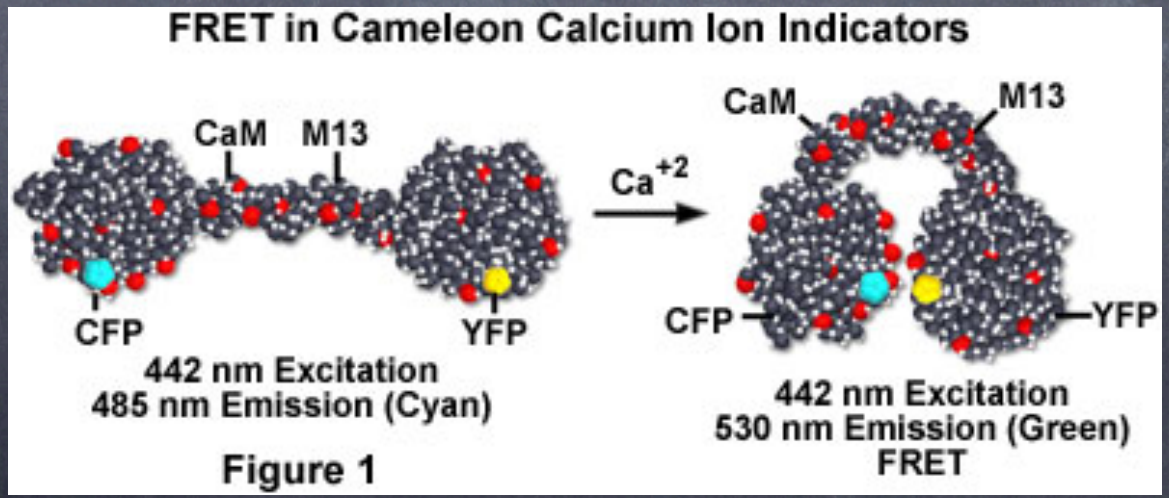

camgaroo

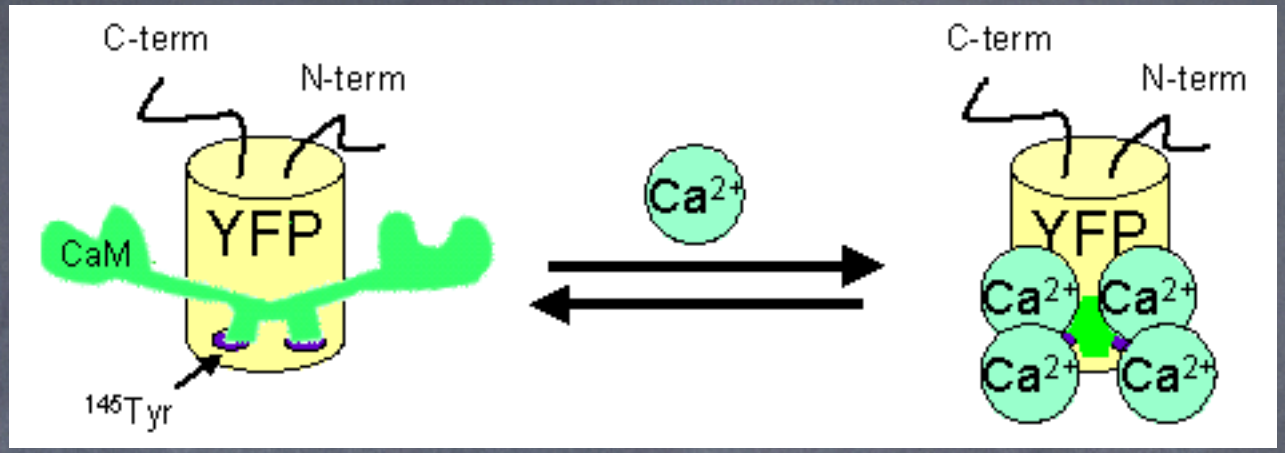

pericam

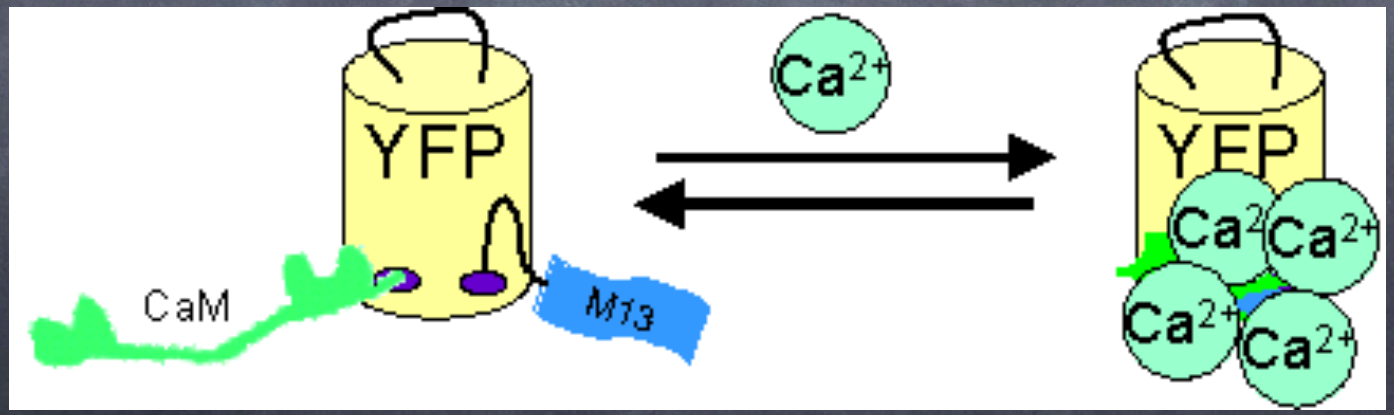

Neuron, Vol. 26, 583–594, June, 2000, Copyright ©2000 by Cell Press

Optical Imaging of Calcium Transients in Neurons and Pharyngeal Muscle of *C. elegans*

Rex Kerr,* Varda Lev-Ram,§ Geoff Baird,†
Pierre Vincent,§# Roger Y. Tsien,‡§
and William R. Schafer*‖
*Department of Biology
†Biomedical Sciences Graduate Program
‡Howard Hughes Medical Institute
§Department of Pharmacology
University of California, San Diego
La Jolla, California 92093

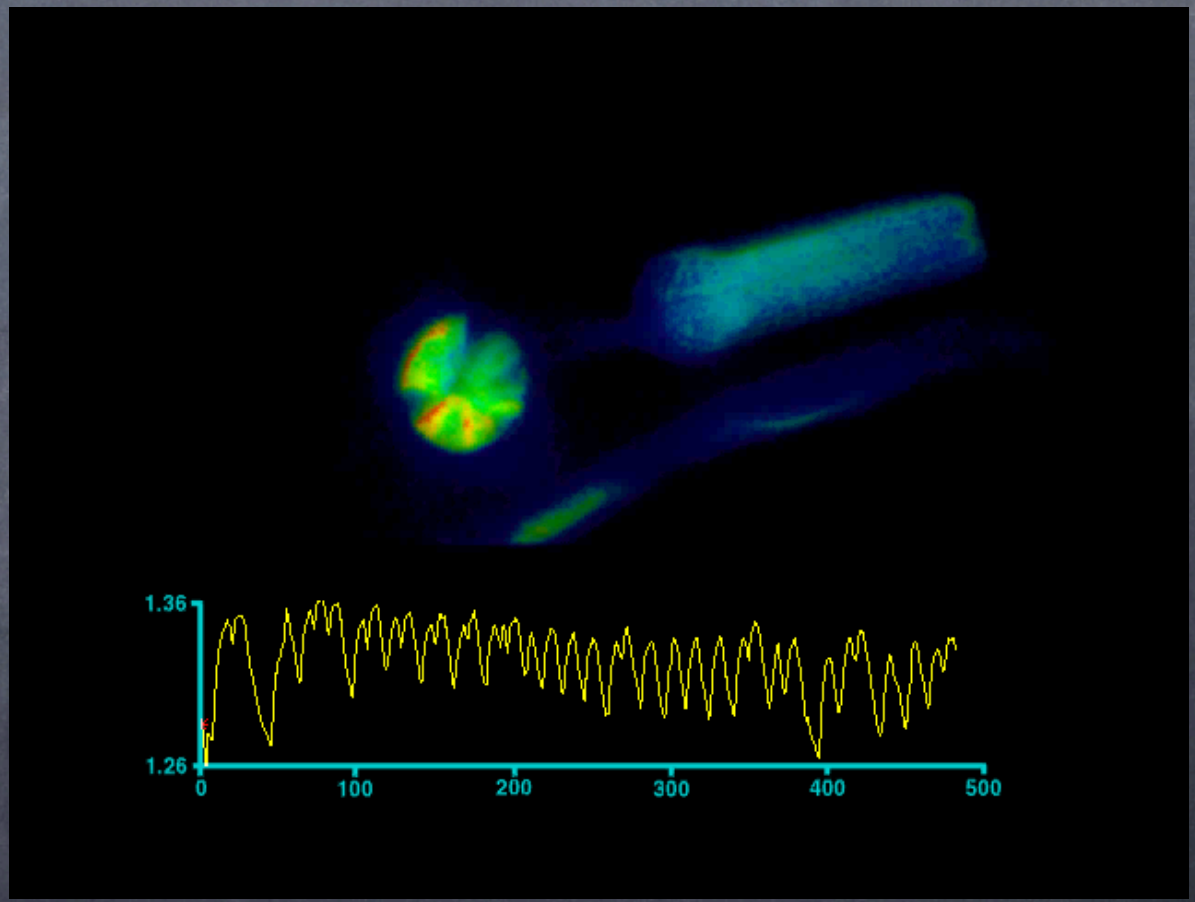

Different strategies to monitor cAMP

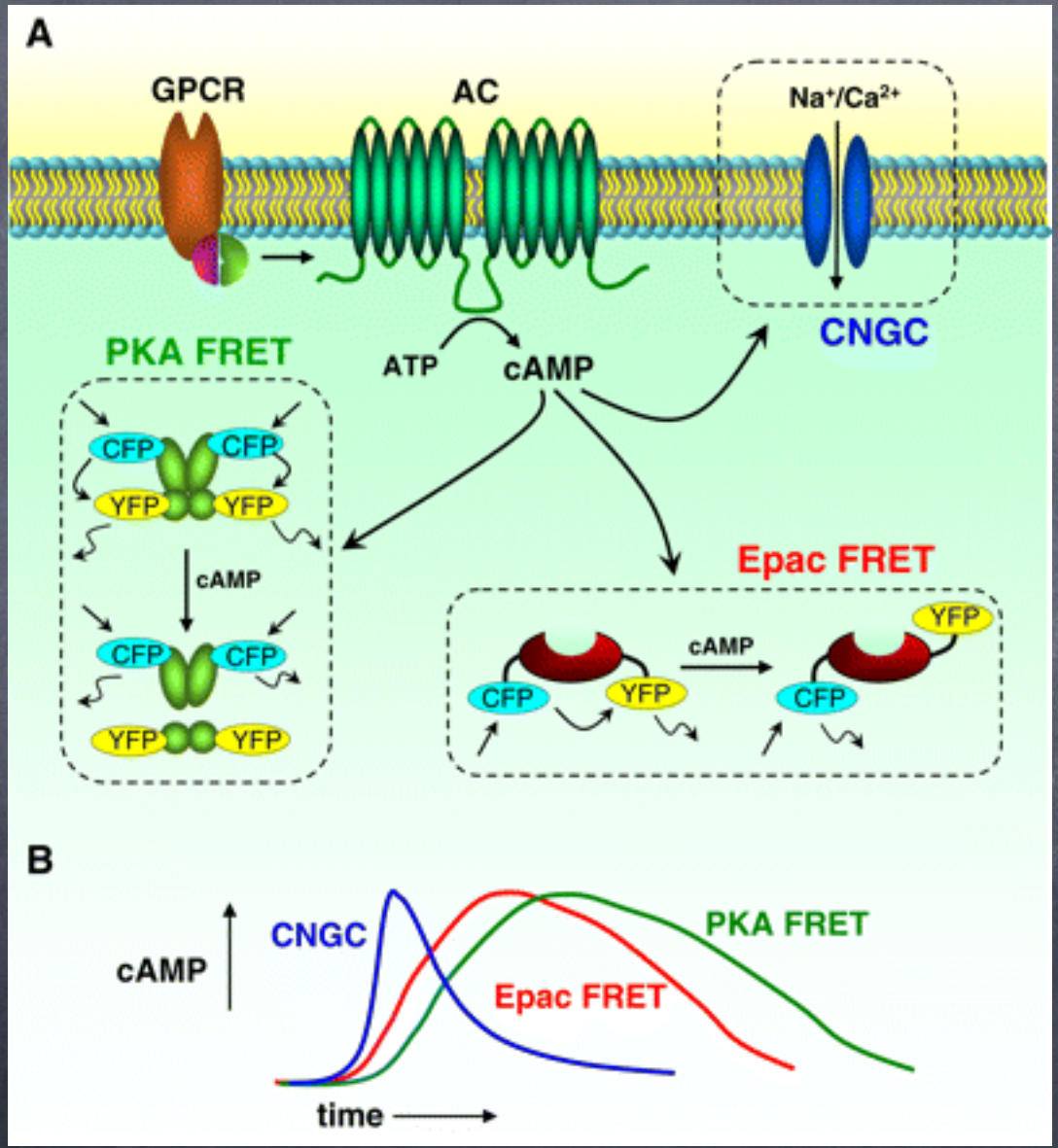

PROTOCOL

FRET measurements of intracellular cAMP concentrations and cAMP analog permeability in intact cells

Sebastian Börner[1,2], Frank Schwede[3], Angela Schlipp[1,2], Filip Berisha[1,2], Davide Calebiro[1,2], Martin J Lohse[1,2] & Viacheslav O Nikolaev[1,2,4]

NATURE PROTOCOLS | VOL.6 NO.4 | 2011 | 427

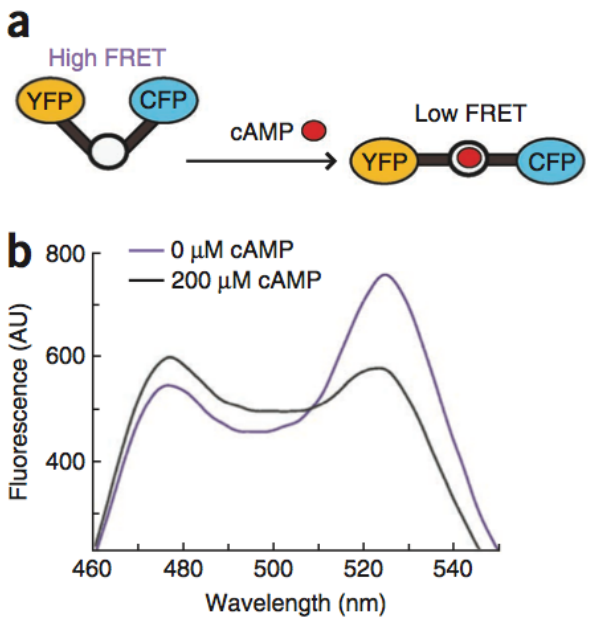

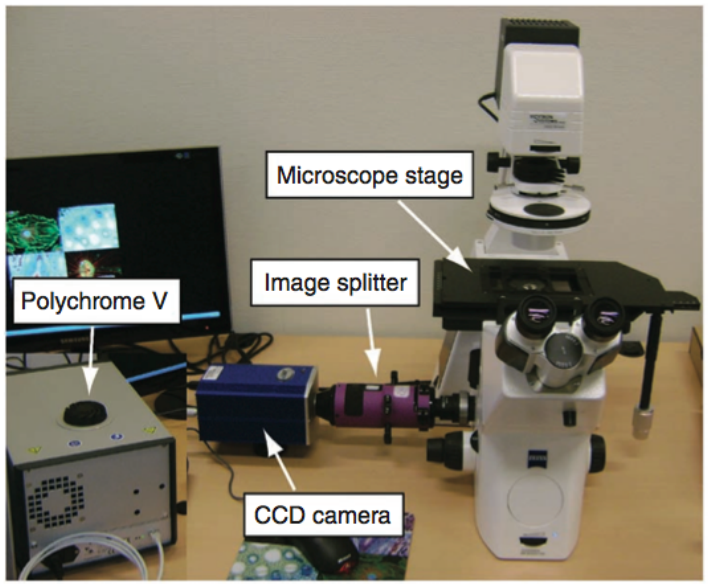

Figure 1 | Schematic structure of the cAMP sensor Epac1-camps and equipment setup for FRET imaging. (**a**) This sensor consists of a single cAMP binding site (encompassing amino acids E157–E316) from human Epac1 protein flanked by YFP and CFP. Binding of cAMP to the sensor leads to a conformational change and a decrease of FRET signal, which is characterized by a concomitant decrease in YFP and an increase in CFP fluorescence. (**b**) Fluorescent spectra of Epac1-camps measured *in vitro* before and after addition of cAMP. (**c**) Layout of the experimental setup that we use for FRET imaging. All principal components are labeled and described in the EQUIPMENT SETUP section.

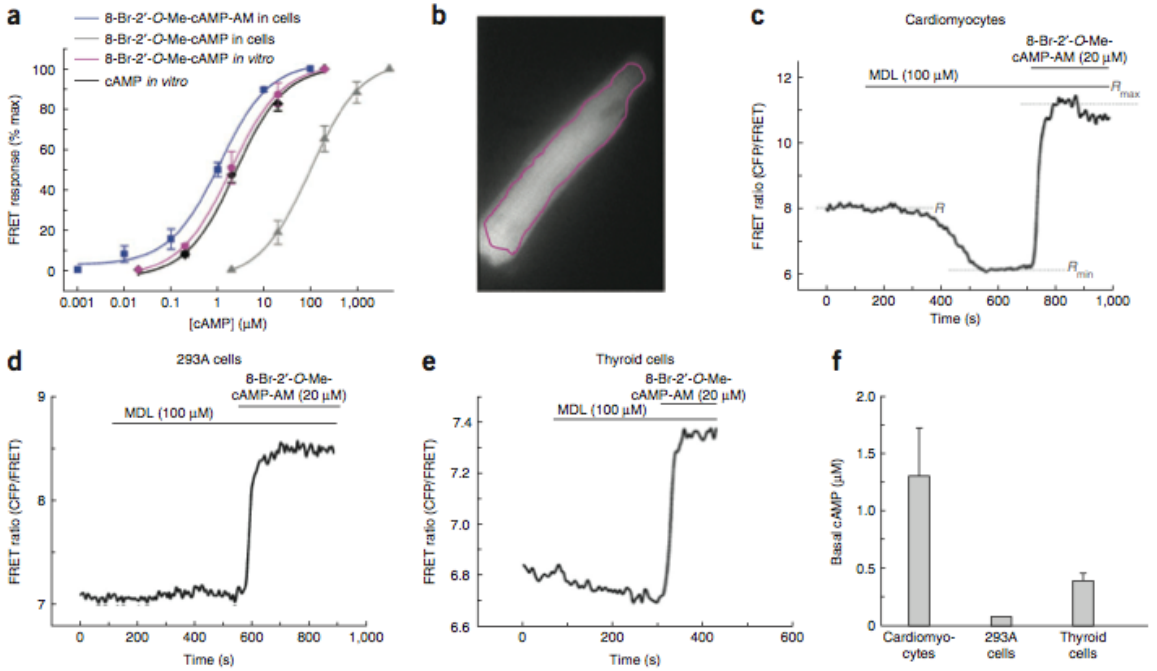

Figure 2 | Measurements of basal cAMP concentrations in various cell types. (**a**) Calibration of Epac1-camps *in vitro* and in 293A cells using cAMP, 8-Br-2′-*O*-Me-cAMP and 8-Br-2′-*O*-Me-cAMP-AM at different concentrations. Mean-normalized FRET values ± s.e.m. (n = 4–5) are shown. Sigmoidal fit of the curves is used to determine EC_{50} and Hill coefficient values. For cAMP, they were 2.5 ± 0.6 μM and 0.74 ± 0.12 μM, respectively. EC_{50} value for 8-Br-2′-*O*-Me-cAMP *in vitro* was 1.6 ± 0.3 μM. However, the concentration-response curve for 8-Br-2′-*O*-Me-cAMP measured in cells is shifted to the right, whereas for 8-Br-2′-*O*-Me-cAMP-AM, it was shifted to the left because of accumulation of this analog in cells (EC_{50} values were 0.95 ± 0.14 μM for 8-Br-2′-*O*-Me-cAMP-AM and 98 ± 40 μM for 8-Br-2′-*O*-Me-cAMP, means ± s.e.m., n = 4). (**b**) Fluorescence image of a cardiomyocyte used in this FRET experiment showing a region of interest over the whole cell that has been selected to monitor CFP/YFP emission intensities and FRET ratio over time. (**c**–**e**) Representative examples of the measurements of basal cAMP concentrations in cardiomyocytes, and 293A and thyroid cells. R_{min} values were determined by inhibition of adenylyl cyclase with 100 μM MDL-12,330A (MDL), and R_{max} values were measured after addition of 8-Br-2′-*O*-Me-cAMP-AM. Cardiomyocytes have high basal cAMP values, whereas 293A cells show virtually no response to MDL, suggesting that basal cAMP values in these cells are ≤100 nM (lower sensitivity range of the Epac1-camps sensor). (**f**) Basal cAMP concentrations in the three types of cells calculated from several experiments (similar to those shown in panels **c**–**e**) using the equation described in **Box 1**. Data are shown as means ± s.e.m. (n = 4–6). Animal procedures were performed with permission from local governmental regulatory authorities.

Published July 29, 2013

JCB: Report

The inner and outer compartments of mitochondria are sites of distinct cAMP/PKA signaling dynamics

Konstantinos Lefkimmiatis,[1,2] Daniela Leronni,[1,2] and Aldebaran M. Hofer[1,2]

[1]VA Boston Healthcare System and [2]Department of Surgery, Brigham and Women's Hospital, Harvard Medical School, West Roxbury, MA 02132

Cyclic AMP (cAMP)-dependent phosphorylation has been reported to exert biological effects in both the mitochondrial matrix and outer mitochondrial membrane (OMM). However, the kinetics, targets, and effectors of the cAMP cascade in these organellar domains remain largely undefined. Here we used sensitive FRET-based sensors to monitor cAMP and protein kinase A (PKA) activity in different mitochondrial compartments in real time. We found that cytosolic cAMP did not enter the matrix, except during mitochondrial permeability transition. Bicarbonate treatment (expected to activate matrix-bound soluble adenylyl cyclase) increased intramitochondrial cAMP, but along with membrane-permeant cAMP analogues, failed to induce measureable matrix PKA activity. In contrast, the OMM proved to be a domain of exceptionally persistent cAMP-dependent PKA activity. Although cAMP signaling events measured on the OMM mirrored those of the cytosol, PKA phosphorylation at the OMM endured longer as a consequence of diminished control by local phosphatases. Our findings demonstrate that mitochondria host segregated cAMP cascades with distinct functional and kinetic signatures.

Intracellular microdomains

Interactions Between Calcium and cAMP Signaling

A.M. Hofer*

VA Boston Healthcare System and the Department of Surgery, Brigham and Women's Hospital and Harvard Medical School, 1400 VFW Parkway, West Roxbury, Massachusetts 02132, USA

Abstract: The calcium ion is quite possibly the single most pervasive signaling molecule used by living organisms for the purpose of communicating internal and external states. It differs from other messengers in that it is neither created nor destroyed, but just moved around inside and outside the cell *via* transporters, pumps and channels to alter its concentration in specific cellular locations. These changes in free [Ca^{2+}] are then detected by a wide array of Ca^{2+}-binding effector proteins whose affinities are appropriately tuned to respond to a particular type of [Ca^{2+}] change. This deceptively simple paradigm dominates the function of many cell types, for example in driving contraction of muscle, action potential generation in nerves, fluid, hormone, and enzyme secretion in secretory cells, and certain immune responses. However, the Ca^{2+} signal does not work in strict isolation, but rather is fine-tuned by many other signals, not the least of which is the other major second messenger, cyclic AMP (cAMP). Conversely, the cAMP pathway is subject to modification by the calcium signal and its various effectors at many different levels. These two fundamental second messengers, used throughout eukaryotes and even prokaryotes, are thus inextricably intertwined. The purpose of the present article is to provide an update on some of the recently described forms of reciprocal regulation between Ca^{2+} and cAMP signaling circuits, with emphasis on interactions that take place in localized domains of the cell.

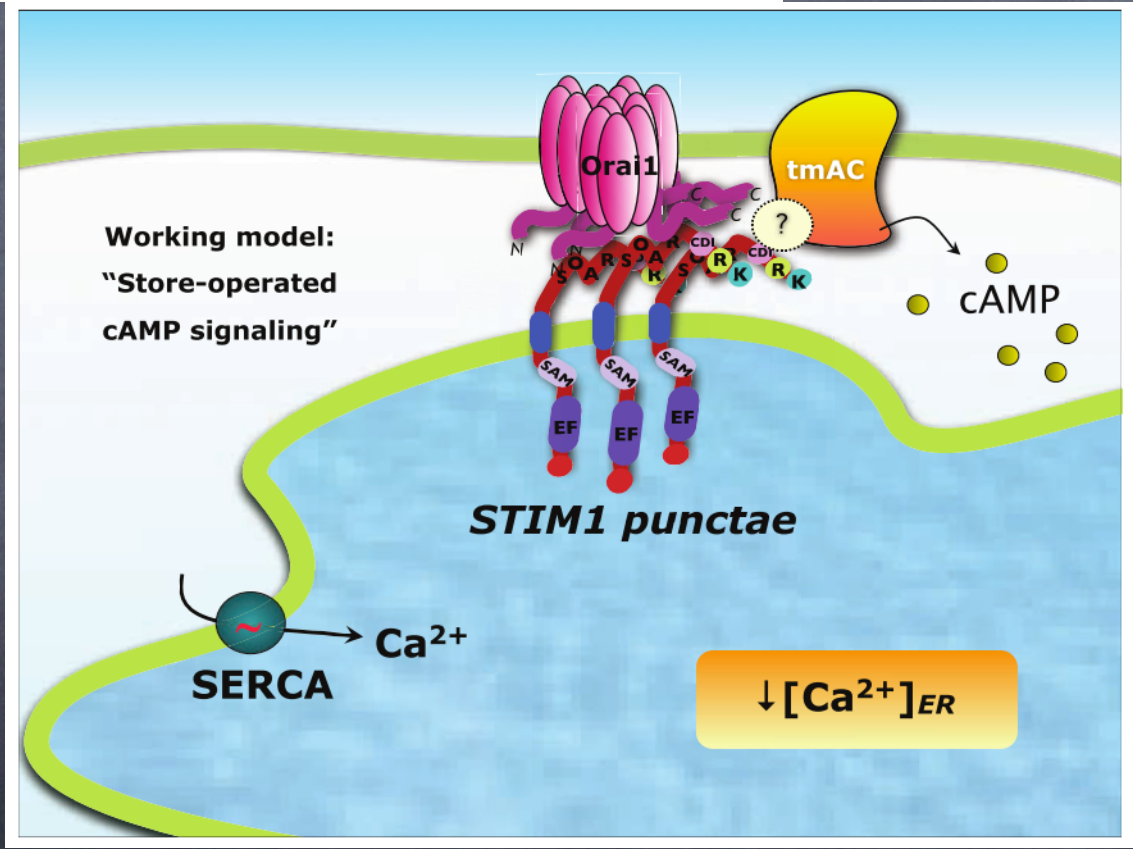

Fig. (1). Model depicting hypothetical mechanism for store-operated cAMP signaling. Lowering of free [Ca^{2+}] within the endoplasmic reticulum causes clustering of STIM1 into "punctae" in zones of the endoplasmic reticulum (ER) that are closely apposed to the plasma membrane. This permits interactions between the "SOAR" (or "CAD") domains of STIM1 and Ca^{2+} permeable Orai channels in the plasma membrane, leading to the well-described phenomenon of store-operated Ca^{2+} entry. In certain cell types, formation of STIM1 punctae following loss of ER Ca^{2+} stores is also somehow connected to activation of conventional transmembrane adenylyl cyclases (tmAC). This latter process does not require Orai1. It is not yet known whether direct binding between STIM1 and tmACs takes place, if or accessory proteins are required for this store-dependent tmAC activation.

nature cell biology

Store-operated cyclic AMP signalling mediated by STIM1

Konstantinos Lefkimmiatis[1], Meera Srikanthan[1], Isabella Maiellaro[1,3], Mary Pat Moyer[2], Silvana Curci[1] and Aldebaran M. Hofer[1,4]

Depletion of Ca^{2+} from the endoplasmic reticulum (ER) results in activation of plasma membrane Ca^{2+} entry channels. This 'store-operated' process requires translocation of a transmembrane ER Ca^{2+} sensor protein, stromal interaction molecule 1 (STIM1), to sites closely apposed to Ca^{2+} channels at the cell surface. However, it is not known whether a reduction in Ca^{2+} stores is coupled to other signalling pathways by this mechanism. We found that lowering the concentration of free Ca^{2+} in the ER, independently of the cytosolic Ca^{2+} concentration, also led to recruitment of adenylyl cyclases. This resulted in enhanced cAMP accumulation and PKA activation, measured using FRET-based cAMP indicators. Translocation of STIM1 was required for efficient coupling of ER Ca^{2+} depletion to adenylyl cyclase activity. We propose the existence of a pathway (store-operated cAMP signalling or SOcAMPS) in which the content of internal Ca^{2+} stores is directly connected to cAMP signalling through a process that involves STIM1.

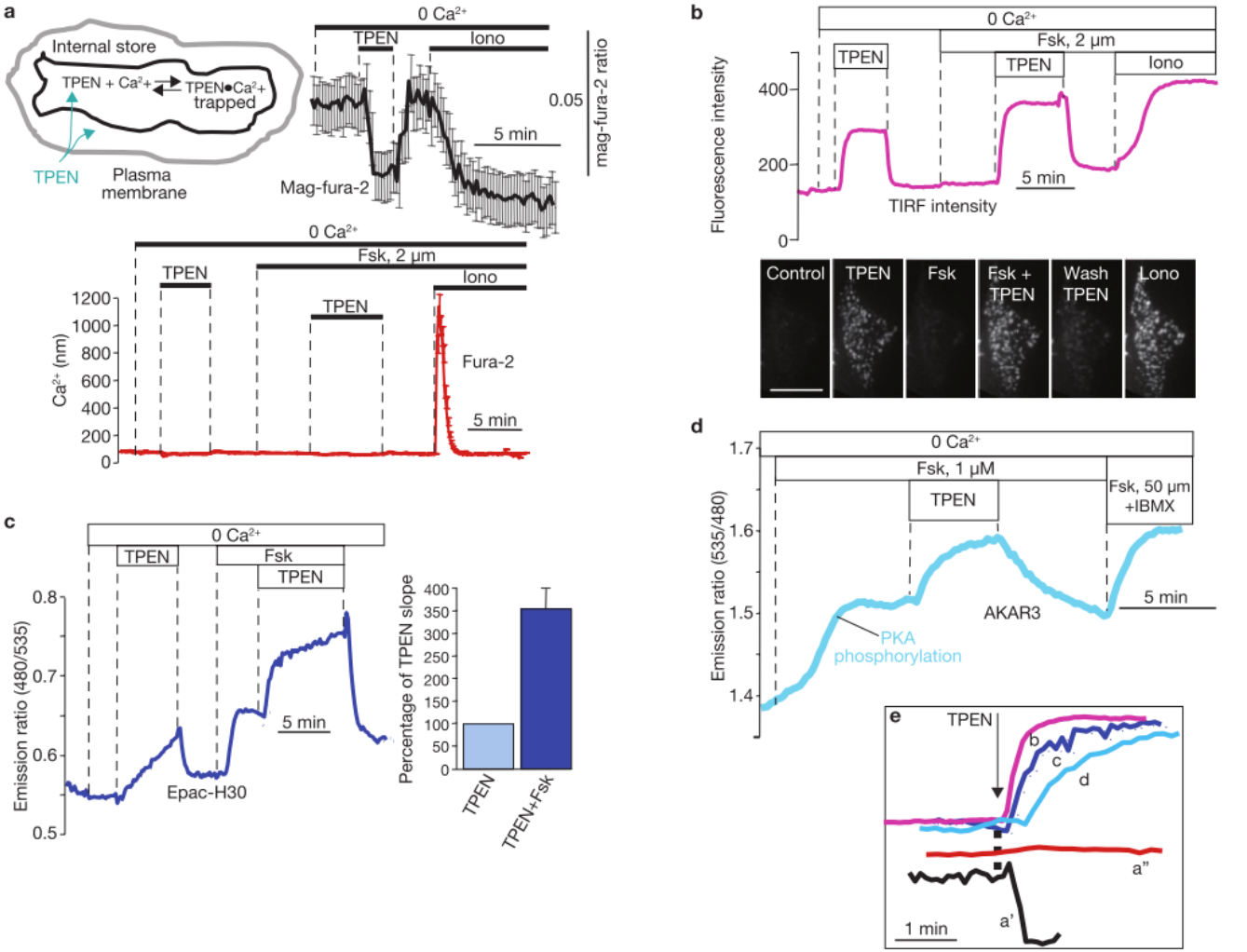

Figure 1 Chelation of Ca^{2+} within internal stores of NCM460 cells induces STIM1 translocation, cAMP signalling and PKA phosphorylation. (**a**) 345 nm/385 nm excitation ratio of compartmentalized mag-fura-2 in intact cells bathed in Ca^{2+}-free solutions (black trace, top upper panel) showing a rapidly reversible effect of TPEN (1 mM) on intraluminal Ca^{2+}. Addition of ionomycin (Iono, 5 μM) caused even further loss of stored Ca^{2+}. Data are mean ± s.e.m. of 9 cells. Cytosolic Ca^{2+} levels (measured by fura-2, red trace, lower panel) did not change during TPEN treatment in Ca^{2+}-free solutions (Fsk, forskolin). The large Ca^{2+} peak elicited by Iono is shown for comparison. Data are mean ± s.e.m. of 36 cells. (**b**) Time course of YFP–STIM1 translocation to the cell surface following treatment with TPEN (1 mM) as measured using TIRF microscopy (upper panel; $n = 16$ cells, 6 experiments). The lower panels show TIRF images of punctae in cells with the indicated treatments corresponding to those shown in the upper panel. Scale bar, 15 μm. (**c**) NCM460 cells expressing Epac-based cAMP sensor. Addition of TPEN (1 mM) in Ca^{2+}-free solution by itself caused an increase in the 480 nm/535 nm FRET emission ratio but this response was markedly potentiated in the presence of Fsk (2 μM). Low concentrations of TPEN (10–40 μM) did not affect the FRET ratio, making a role for heavy metals in this process unlikely. The inset shows summary data (mean ± s.e.m. of 47 cells in 6 experiments) for the relative rate of TPEN responses in the presence and absence of forskolin. (**d**) 535 nm/480 nm FRET emission ratio of the PKA phosphorylation sensor, AKAR3, after treatment with TPEN (representative of 10 cells in 7 independent experiments). At the end of most experiments, cells were stimulated with saturating concentrations of the PDE inhibitor isobutylmethyl xanthine (IBMX, 1 mM) and Fsk (25–50 μM) to establish the maximum ratio response. (**e**) Overlay of time courses of TPEN responses in the presence of forskolin from experiments in **a**–**d** for mag-fura-2 (**a**′), fura-2 (**a**′′), YFP–STIM1 TIRF (**b**), Epac-H30 (**c**) and AKAR-3 (**d**).

Genetically encoded fluorescent reporters of protein tyrosine kinase activities in living cells

Alice Y. Ting*, Kristin H. Kain†, Richard L. Klemke†, and Roger Y. Tsien*‡§

PNAS | December 18, 2001 | vol. 98 | no. 26 | 15003–15008

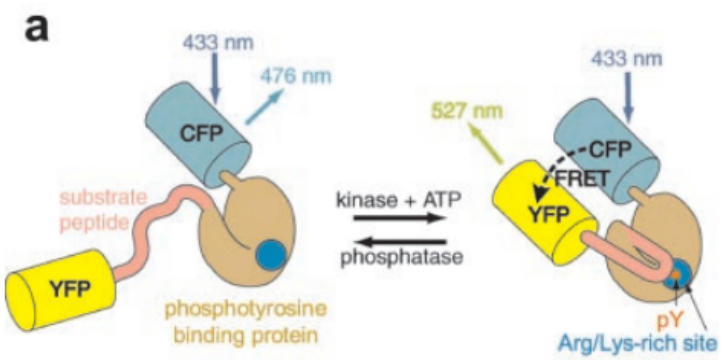

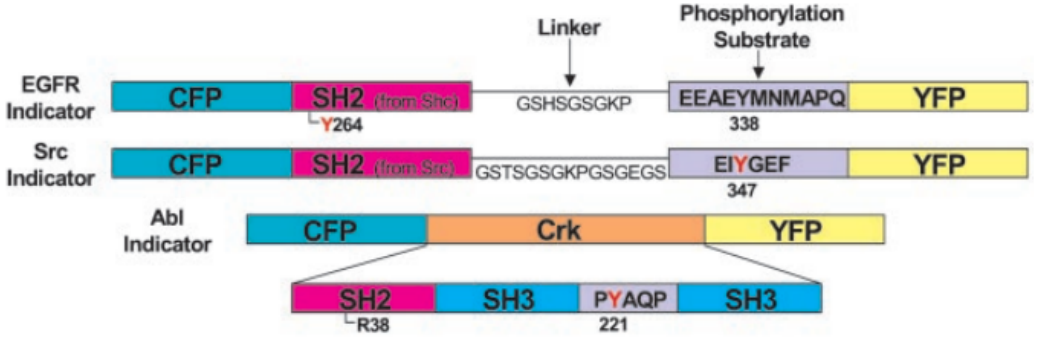

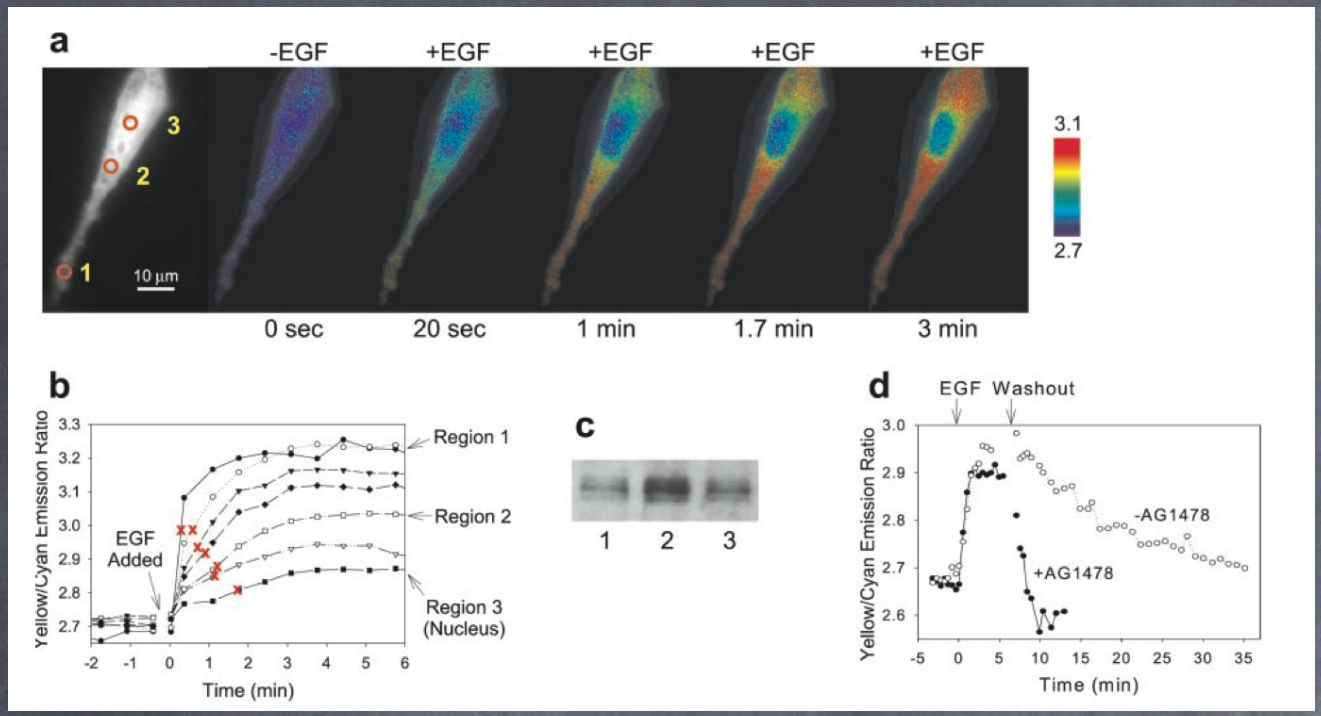

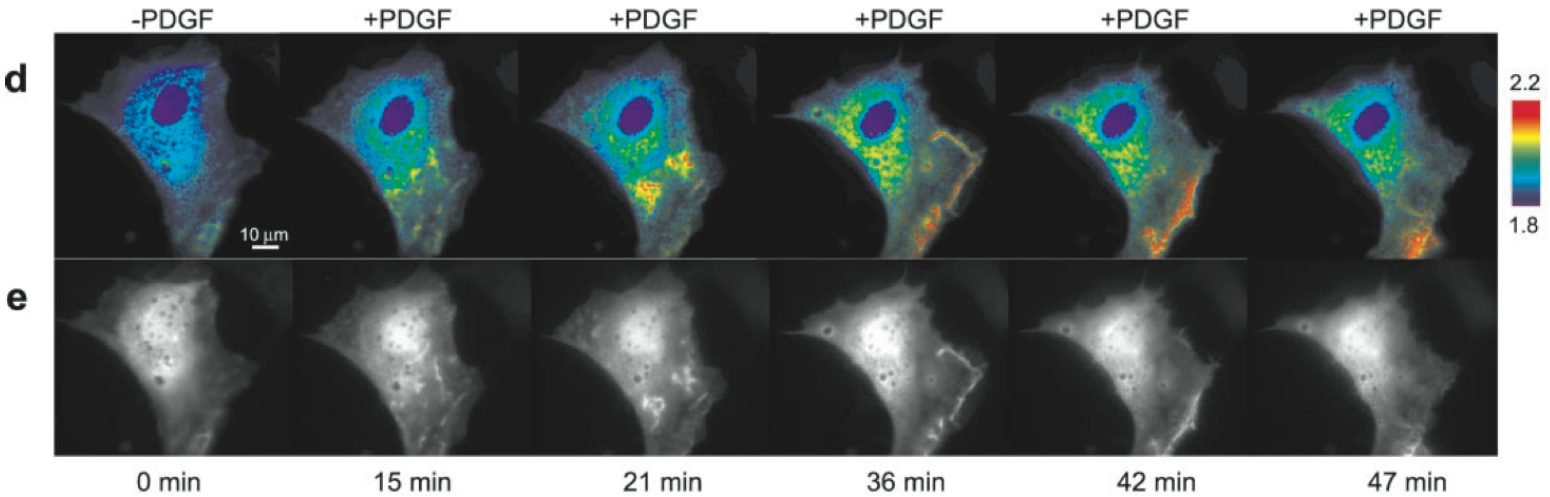

Fig. 3. Cellular response of the Crk-based reporter. Wild-type MEFs stimulated with H_2O_2 displayed a FRET increase in the cytosol over 20 min but no change in the nucleus (*a*). Null cells did not display such an increase. An antiphospho-Y221Crk Western blot of crude cell lysates from NIH 3T3 cells transfected with the Crk-based indicator shows an increase in phosphorylation of the indicator on PDGF stimulation (*b*). Phosphorylation is suppressed by pretreating cells with the Abl inhibitor STI-571. The emission ratio time course (*c*) for different regions of the PDGF-stimulated cell depicted in *d* shows a cytoplasmic increase in FRET followed by a dramatic FRET increase within the PDGF-induced membrane ruffles. Corresponding images of the YFP fluorescence show that the Abl reporter concentrates in the membrane ruffles (*e*).

Biochimica et Biophysica Acta 1834 (2013) 1387–1395

Contents lists available at SciVerse ScienceDirect

Biochimica et Biophysica Acta

journal homepage: www.elsevier.com/locate/bbapap

Review

Fluorescent biosensors — Probing protein kinase function in cancer and drug discovery☆

May C. Morris *

Chemical Biology and Nanotechnology for Therapeutics, CRBM-CNRS-UMR5237,1919 Route de Mende, 34293 Montpellier, IFR122, France

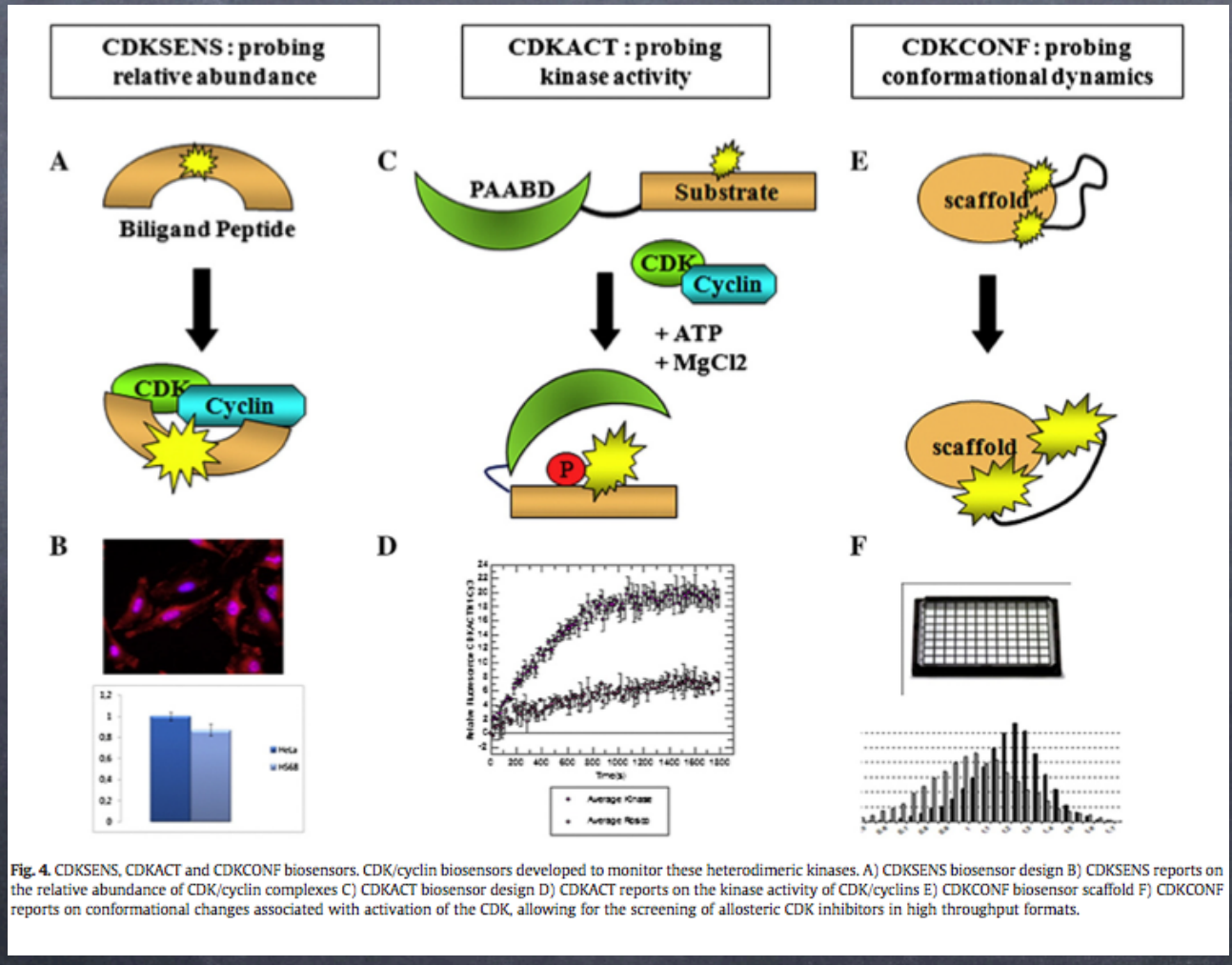

Fig. 4. CDKSENS, CDKACT and CDKCONF biosensors. CDK/cyclin biosensors developed to monitor these heterodimeric kinases. A) CDKSENS biosensor design B) CDKSENS reports on the relative abundance of CDK/cyclin complexes C) CDKACT biosensor design D) CDKACT reports on the kinase activity of CDK/cyclins E) CDKCONF biosensor scaffold F) CDKCONF reports on conformational changes associated with activation of the CDK, allowing for the screening of allosteric CDK inhibitors in high throughput formats.

Biosensors are useful tools for drug discovery applications

- Drug Discovery Programmes : HTS & HCS
- Positional, FRET, Intensity-based biosensors
- Multiparametric Screens
- Postscreen validation of hits
- Characterization and Optimization of leads
- Preclinical Evaluation of Drugs

(biodistribution, pharmacokinetics, response)

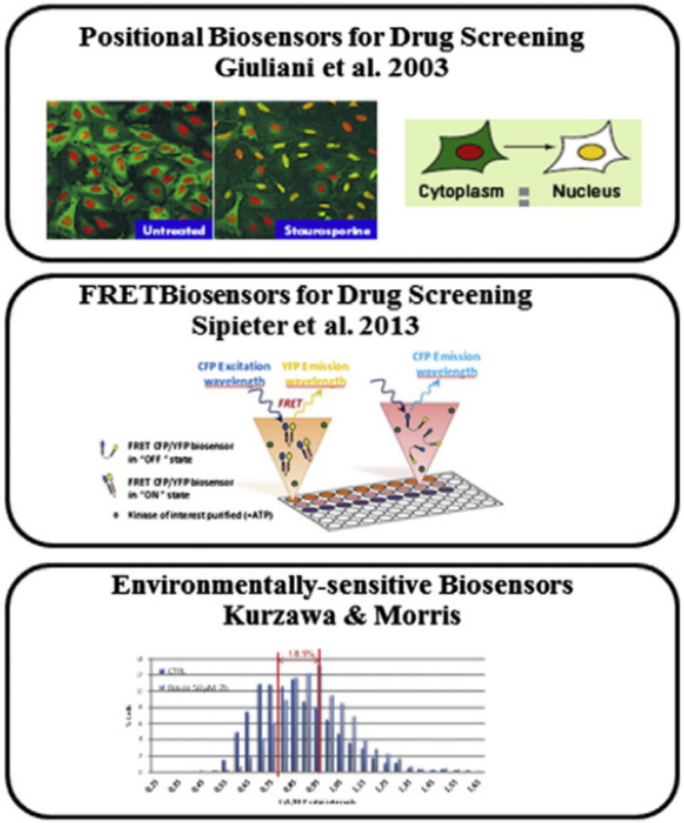

Fig. 6. Biosensors in drug discovery. Fluorescent biosensors are widely used in drug discovery programs for the identification of drugs by HTS, HCS approaches, for postscreening evaluation of hits, optimization of leads, preclinical evaluation and clinical validation of candidate drugs.

FRET-based biosensors for protein kinases: illuminating the kinome

Jin Zhang*[a] and Michael D. Allen[b]

Mol. BioSyst., 2007, **3**, 759–765 | 759

High throughput use of FRET:
biosensors/chips to test enzymatic activity

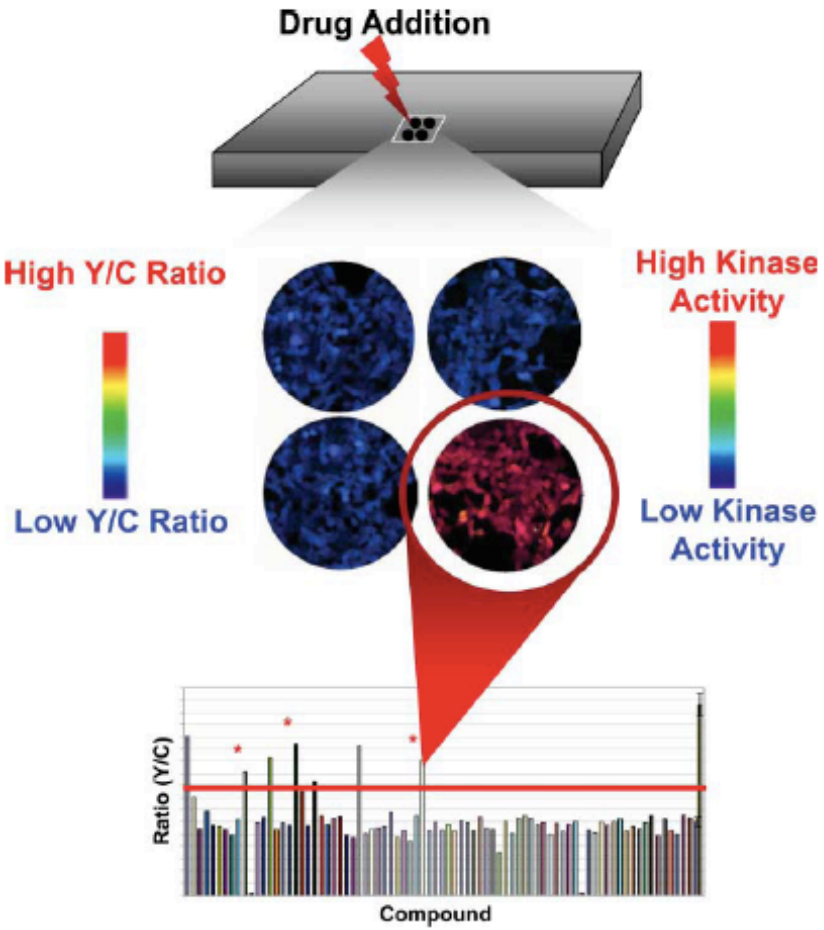

Fig. 2 Schematic representation of the application of kinase biosensors in live-cell, high throughput screens for novel pathway modulators. Individual compounds are added to each well of the microtiter plates, which contain living mammalian cells expressing a kinase biosensor. Cyan and yellow fluorescence intensities are read by a fluorescence plate reader and emission ratios are calculated to detect which wells contain compounds that may activate or inhibit the kinase. High yellow/cyan (Y/C) emission ratios (red) represent potential agonists.

Table 1 FRET-based kinase activity reporters (KAR) that utilize the modular design of a phosphoamino acid binding domain and kinase-specific substrate as the molecular switch

Reporter	Target	FRET pair	Signal change (%)[a]	Reference
AKAR	PKA	ECFP/cpVenus	40 ↑	13,20,28,47
Aktus	PKB	CFP/YFP	10 ↑	17
ATOMIC	ATM kinase	CFP/YFP	10 ↓	21
BKAR	PKB	ECFP/Citrine	10–25 ↓	18
CKAR	PKC	ECFP/Citrine	15–20 ↓	16
CrkII-based reporter	Abl	ECFP/Citrine	15–30 ↑	14
DKAR	PKD	CFP/YFP	10–20 ↓	22
EGFR reporter	EGFR	ECFP/Citrine	25–35 ↑	14
Erkus	Erk1	CFP/YFP	10 ↓	24
Phocus	IR	CFP/YFP	15–20 ↑	15
Picchu	Abl/EGFR	CFP/YFP	60 ↑	23
Src reporter	Src	ECFP/Citrine	30–35 ↓	14,19

[a] Best dynamic ranges are shown when different generations of reporters exist, with arrows representing the directions of FRET responses when plotted as changes in yellow over cyan emission ratio.